Norden, B., Förster, A., Balling, N. (2008): Heat Flow and lithospheric thermal regime in the Northeast German Basin. - Tectonophysics, 460, 1-4, 215-229

DOI: 10.1016/j.tecto.2008.08.022

Heat flow and lithospheric thermal regime in the Northeast German Basin

Ben Norden[1], Andrea Förster[1], Niels Balling[2]

[1] GFZ German Research Centre for Geosciences, Section 5.2 Geothermics, Telegrafenberg, 14473 Potsdam, Germany.

[2]University of Aarhus, Department of Earth Sciences, Hoegh-Guldbergs Gade 2 DK-8000 Aarhus C, Denmark.

Corresponding author: B. Norden, Tel. 0049-331-288-1578, Fax. 0049-331-288-1540

Abstract

New values of surface heat flow are reported for 13 deep borehole locations in the Northeast German Basin (NEGB) ranging from 68 to 91 mW m^{-2} with a mean of 77 ± 3 mW m^{-2}. The values are derived from continuous temperature logs, measured thermal conductivity, and log-derived radiogenic heat production. The heat-flow values are supposed free of effects from surface palaeoclimatic temperature variations, from regional as well as local fluid flow and from thermal refraction in the vicinity of salt structures and thus represent unperturbed crustal heat flow. Two-D numerical lithospheric thermal models are developed for a 500 km section along the DEKORP-BASIN 9601 deep seismic line across the basin with a north-eastward extension across the Tornquist Zone. A detailed conceptual model of crustal structure and composition, thermal conductivity, and heat production distribution is developed. Different boundary conditions for the thickness of thermal

lithosphere were used to fit surface heat flow. The best fit is achieved with a thickness of thermal lithosphere of about 75 km beneath the NEGB. This estimate is corroborated by seismological studies and somewhat less than typical for stabilized Phanerozoic lithosphere. Modelled Moho temperatures in the basin are about 800 °C; heat flow from the mantle is about 35 to 40 mW m^{-2}. In the southernmost part of the section, beneath the Harz Mountains, higher Moho temperatures up to 900 to 1000 °C are shown. While the relatively high level of surface heat flow in the NEGB obviously is of longer wave length and related to lithosphere thickness, changes in crustal structure and composition are responsible for short-wave-length anomalies.

Key words: Northeast German Basin, heat flow, thermal modelling, thermal structure, thermal lithosphere.

1. Introduction

In recent years, the Northeast German Basin (NEGB, Fig. 1) has been subject of renewed interest for studying heat flow and the crustal and lithosphere structure. The principal aim of this study is to report new surface heat flow (q_s) data for the NEGB and to combine these values with the wealth of recent information from different seismic, seismologic and other geophysical studies to generate a consistent lithospheric thermal model. The paper (1) presents new q_s values determined at 13 borehole sites based on continuous temperature logs and recent measurements of thermal properties,

(2) provides estimates on mantle heat flow (q_m) by accounting for the radiogenic heat production within the crust, (3) develops a numerical model of the lithospheric thermal structure, (4) investigates the sensitivity of parameter changes, including thickness of thermal lithosphere, to temperature and heat-flow distribution and (5) discusses implications for the geodynamic state of the basin.

Three-dimensional thermal models down to the Moho were made by Scheck (1997) and Bayer et al. (1997) for the NEGB. The thermal parameters used for the sedimentary sequence reflect the state of knowledge at that time. The boundary conditions of the model were either a fixed Moho temperature (600 °C) or a fixed Moho heat flow (25 mW m^{-2}). The crustal domain below the sediments was simplified to a block model, in which thermal conductivity (λ) and radiogenic heat production (A) decrease linearly to a depth of 30 km. No lateral compositional variations were considered for the crust. These models were slightly modified by Ondrak et al. (1998) by varying locally the input parameters for the crust and the boundary conditions of the model to attain a better fit to measured borehole temperature profiles.

Other published thermal models of the NEGB consider a coupled temperature and burial history, calibrated by organic-maturity parameters and temperature recordings in boreholes and with heat-flow values below the sedimentary veneer used as a boundary condition (Friberg et al., 2000, Friberg, 2001). Vosteen et al. (2004) estimated the present-day heat-flow distribution at 6 km

depth in the basement across the NEGB using inverse modelling of the steady-state conductive thermal regime based on λ, A, and borehole temperature information.

At lithospheric scale, Marotta et al. (2000) present lithosphere strength profiles and a 2-D flexural model along the BASIN 9601 seismic line including a general steady-state thermal model with 1600 K at about 80 km depth as the constant lower thermal boundary condition and no lateral variations in the thermal properties of the crust. Gemmer et al. (2003) modelled the late Cretaceous-Cenozoic evolution of the North German Basin in a general 3D thermomechanical numerical model in which vertical movements caused by lithospheric compression and stress relaxation played a dominant part.

The present paper fills a gap by investigating the thermal regime of the crust and upper mantle beneath the NEGB using modelling procedures similar to those used for adjacent areas, such as along a transect from the southern part of the Baltic Shield across the Sorgenfrei-Tornquist Zone (STZ) and the Caledonian Deformation Front (CDF) into the Northwest German Basin (NWGB) (Balling, 1995) and across Poland including the Polish Basin to the east (Majorowicz et al., 2003; Majorowicz, 2004).

2. Geological setting and geodynamic evolution

The NEGB is part of the mid-European basin system formed in Permian time south of the Tornquist Zone (e.g. Ziegler, 1990; Glennie, 1998). The basin is connected to the west with the NWGB and to the east with the Polish Basin (PB) (Fig.1). These basins formed part of a regional Southern Permian Basin.

The basement of the NEGB is comprised of rocks of variable composition and age (Katzung and Ehmke, 1993; references therein) pertaining in the south to the Variscan belt (folded Namurian and older units) and in the north to the Variscan foredeep. Whereas in the southern part of the Variscan foredeep the Namurian to Westphalian rocks were deformed during the Variscan orogeny, Namurian to Stephanian sediments in the northern part of the foredeep remained unaffected. The Carboniferous and Devonian rocks of the foredeep discordantly overlie basement units that were either folded in Caledonian time (northern part) or consolidated in earlier times (southern part). Meissner et al. (1994) termed the northern part of the Variscan foredeep, south of the Caledonian Front, (East) Avalonia (Fig. 1). It is a microcontinent that originated from the northern rim of Gondwana and joined with Baltica during the Caledonian cycle. Krawczyk et al. (1999) interpreted from the DEKORP-BASIN 9601 line (Fig. 2) the presence of Baltica crust perhaps as far south as the depocenter of the basin (Fig. 3). In general, details of structure and composition of the crust beneath the NEGB are a matter of interpretation and discussion (cf. Bayer et al., 1999; Krawczyk et al., 1999).

Tectonic movements in the late Stephanian have caused activation of preferentially NNE and subordinately NNW- to NW-trending fault systems associated with a Permian−Carboniferous volcanic series that is up to 2000-m-thick and emplaced in pull-apart basins (Benek et al., 1996). These volcanic rocks are subdivided into associations of different composition (e.g., Benek et al., 1995, 1996) for which Norden and Förster (2006) provided thermal properties. Persistent thermal uplift in the late Carboniferous/early Permian time resulted in denudation and a significant hiatus before thermal subsidence and reactivation of the fault systems formed an area, which became increasingly larger and in which first the Lower Permian (Rotliegend) clastics and later the Upper Permian (Zechstein) mudstones and evaporites were deposited. After Permian time, the NEGB was filled with Mesozoic to Cenozoic sediments (e.g. Hoth et al., 1993; Scheck and Bayer, 1999; Scheck-Wenderoth and Lamarche, 2005).

Van Wees et al. (2000) interpret from basin modelling studies the beginning of subsidence of the Southern Permian Basin of central Europe in response to thermal contraction of the lithosphere after the termination of wrench tectonics that was associated with thermal destabilisation of the lithosphere, deep fracturing of the crust, regional uplift, and volcanism. Their tectonic subsidence curves and the distribution of faults indicate that the early Permian ‘event’ was associated with a greater degree of mantle-lithosphere thinning than crustal extension and that thinning was heterogeneous throughout the basin.

A phase of accelerated subsidence commenced in the late Permian as a result of thermal contraction and lasted until the end of the early Triassic. This phase is followed by relatively low subsidence rates from the middle Triassic to early Jurassic. Major rift- and wrench-tectonics in the Triassic, Jurassic, and early Cretaceous in the western and central Europe, entailing a renewed destabilization of the lithosphere, had little effect on the North German platform. The lithosphere had apparently to a large degree stabilized towards the end of the Cretaceous to thicknesses of some 100−120 km (Ziegler et al., 1995). This thermal stabilization also is concluded from the fact that late Triassic-early Cretaceous stretching/rifting events in Europe (Ziegler et al., 1995) affected the NEGB only by formation of local NNE-SSW-directed depocenters (e.g. the Rheinsberg Trough) and did not result in large-scale increased (thermal) subsidence (Scheck, 1997; Scheck and Bayer, 1999; Scheck-Wenderoth and Lamarche, 2005). Moreover, the basin underwent a differentiation into areas of local subsidence or local uplift partly associated with the movement of Upper Permian (Zechstein) salt and the growth of salt-core anticlines (Kossow et al., 2000).

The late Cretaceous and Paleocene compressional/transpressional intra-plate deformation in the Alpine foreland of Europe (Ziegler et al., 1995) also affected the NEGB. However, in contrast to areas to the west (e.g. the Lower Saxony Basin) and the Polish Trough to the east, which both inverted at that time, the NEGB was only moderately affected. Only the TTZ (Fig. 1) to the

north and the Elbe Zone, bordering the NEGB to the south, experienced large-scale inversion by uplift along thrust faults (Kossow and Krawczyk, 2002). In the basin, some local highs were developed leaving marginal troughs between them. A final subsidence phase in the Cenozoic, and some associated general increase in sediment accumulation is observed in the western part of basin (Scheck and Bayer, 1999; Scheck-Wenderoth and Lamarche, 2005), which seems related to a renewed cycle of rifting and lithosphere destabilization in central Europe (Ziegler, 1990).

The lithosphere in the Alpine foreland of central Europe is characterized by crustal thicknesses <35 km and lithospheric thicknesses <90 km (Blundell, 1999; references therein), and an upper asthenospheric mantle generally displaying anomalously low-shear wave anomalies associated with high temperatures (Zielhuis and Nolet, 1994a, b; Ziegler et al., 1995; Cloetingh et al., 2005). Although there is a debate with regard to the timing and nature of this anomaly, its development is likely to have caused upward displacement of the lithosphere-asthenosphere boundary and of the lithospheric isotherms, increased heat flow and thus a progressive weakening of the lithosphere (Ziegler et al., 1995; Marotta et al., 2000, 2002; Gemmer et al., 2003).

3. Heat-flow data

According to Fouriers law of heat conduction, heat-flow density (q) is given by the product of temperature gradient (grad T) and thermal conductivity (λ):

$$q = -\lambda \, grad \, T \quad (1)$$

The interval method (Blackwell and Spafford, 1987; Powell et al., 1988) was used to determine (q) at each borehole location. The depth intervals selected depend on drillcore control for the measurements of λ and are mostly in the Permian and pre-Permian formations, at depth of 1500−5000 m (Table 1). Thermal conductivity measured on 363 drillcore samples under ambient conditions is corrected to represent conditions of water saturation and in-situ temperature (Table 1). The corrections are based on equations by Somerton (1992) for sedimentary rocks and by Sekiguchi (1984) for volcanic rocks, respectively. The measurements were done using the optical scanning method (Norden and Förster, 2006; references therein).

Temperatures from continuous logs are available at 50-m intervals (Förster, 2001), except in the GrSk 3/90 borehole, where data with a recording interval of 0.15 m (Hurter, 2002) are used. Temperature gradient versus depth plots helped to select suitable intervals for heat flow calculation. Care has been taken to select intervals that have not experienced intra-borehole fluid flow. Interval temperature gradients (Table 1) are determined by the least-squares fit to the temperature data.

In most cases, the temperature logs reflect quasi steady-state thermal conditions (Förster, 2001; labelled A–C in Table 1). Logs not entirely recovered from drilling perturbation (labelled ‘D’ in Table 1) are corrected

using the empirical approach of Förster (2001) due to the lack of data on drilling and circulation times.

The empirical correction is based on the 'cross-over point' (COP) of temperature perturbation during drilling. During temperature recovery, temperatures above the COP decrease towards thermal equilibrium and below COP they increase, respectively. For the NEGB, the COP can be determined from the empirical relation (Förster, 2001):

$$COP\ [\mathrm{m}] = 0.39\ z\ [\mathrm{m}] + 267 \qquad (2)$$

where z is the total depth of the borehole. Mean temperature gradients are calculated between (1) the surface with a mean temperature of 8 °C and the temperature at COP and (2) temperature at COP and the empirically corrected temperature at the bottom end of the temperature profile. A comparison of these gradients with the gradients calculated by least-squares fits to the measured temperature data allows an estimation of the magnitude of temperature perturbation. Differences in temperature gradients are then used to correct the gradients for the heat-flow intervals (Table 1).

Palaeoclimatic surface temperature changes may penetrate down to a depth of a few kilometres (Beck, 1977; Pollack and Huang, 2000) thus affecting q_s. To account for the perturbations on heat flow, the effect on the temperature gradient (and not the temperature itself) is most important. From the models presented in Figure 4 generally suitable for the conditions of northern Germany, we observe substantial temperature gradient perturbations in the

upper some hundreds of meters. Perturbations are generally negligible at depths >1500-2000 m (see also Powell et al., 1988; Kukkonen and Jõehlet, 2003). The heat-flow intervals used in this study are mostly at depth of >2500—3000 m (Table 1), and so a palaeoclimatic correction is not needed.

In order to determine crustal heat flow free of small-wavelength thermal anomalies originating in the sedimentary cover, q is corrected on one location (RmwL 11A/69, Table 1) for heat refraction associated with salt structures. For a quantification of this effect, which is caused by strong contrast in λ, numerical 2-D and 3-D thermal models are generated. The Gransee area (Fig. 5), containing salt diapirs, salt pillows, and combinations of diapirs and pillows, serves as locus typicus for a 3-D model. The model domain comprises an area of 50 x 50 km and contains 500 x 500 m cells. The base of salt is located at 4500 m depth. The base of the model is at 11 km. General salt thickness in the model is 500 m and varies significantly in the salt structures. Parameters used in the modelling are shown in Table 2. In general, q in the top part of the salt bodies and in the sedimentary section above the salt is higher (by the order of up to 100 mW m^{-2}; salt structures 1−6, Fig. 6A) compared to locations away from structures (margin, Figs. 6B, 6C). Between salt diapirs, q may be weakly decreased (Gs 2/67, Fig. 6B). The modelling shows this effect to be on the order of 2−3 mW m^{-2}. In general, q varies significantly with depth depending on the shape of the salt and on the distance to salt structure. The perturbation on background q is usually restricted to an area within 5−7 km of the salt structure (Fig. 6C). The *RmwL*

11A/69 borehole is located in the middle of an isolated salt wall with a thickness of about 3 km, a situation roughly similar to salt structure number two (Figs. 5 and 6a). The temperature field at this borehole is strongly influenced by heat refraction. According to the modelling, the high q in the *RmwL 11A/69* borehole (observed local heat flow up to 131 ± 13 mW m^{-2}; Table 1) needs a correction in the order of 50−60 mW m^{-2}.

The relatively great depth in the basin at which q is determined, requires assessment of the radiogenic heat (A) generated between the surface and the depth of the heat-flow value. The portion of heat flow (q(A), Table 1) generated in the supra-Permian succession needs to be added to obtain q_s, which is the parameter to be reported in heat-flow studies (Powell et al., 1988) and the observed surface boundary constraint on our lithospheric thermal models. In the NEGB, q(A) amounts to 0.5–2 mW m^{-2} where the succession is fairly thin (500–1500 m, e.g. above salt diapirs and at the northern basin margin), and 4–8 mW m^{-2} where the overburden is about 4 km thick (Norden and Förster, 2006). For the heat-flow sites reported in this paper, q(A) ranges between 0.5 and 6.6 mW m^{-2} (Table 1).

Surface heat flow has been determined at 13 locations in the NEGB (Table 1, Fig. 3). Values range between 68 and 91 mW m^{-2} with a mean value of 77 ± 3 mW m^{-2}. The overall uncertainty of the individual values is estimated to be on the order of up to 10–15 %. In a conduction dominated domain, the relatively high q_s could either be a result of high A values in the crust, leaving the heat

flow from the mantle, q_m at values typical for a stabilized Phanerozoic lithosphere, or be a result of an increased q_m. Different thermal modelling scenarios and their effects on temperature and heat flow were investigated for a lithosphere section along the deep reflection seismic DEKORP-BASIN 9601 line, extended to the northeast using data from the off-shore deep seismic lines PQ2-004, PQ2-005, PQ2-9.1, and DSB-9 (Fig. 2).

4. Heat flow and crustal temperature

4.1 Geotherms

In a first step, steady-state 1-D temperature profiles (geotherms) were calculated using the analytical solution to the heat equation:

$$T_1 = T_0 + \frac{q_0}{\lambda} z - \frac{A}{2\lambda} z^2 \qquad (3)$$

where λ and z are the thermal conductivity and the thickness of the regarded interval; T_0 and T_1 represent the temperature at the top and at the bottom of the interval, respectively. The heat flow at the top of the interval is q_0 and A represents the radiogenic heat production of the interval. For the uppermost interval, T_0 is the mean surface temperature (8 °C). λ is corrected to represent in-situ temperature and pressure conditions (see next sections).

4.1.1 Crustal structure

The geological structure and the nature of the sedimentary formations in the NEGB are well known. Table 3 lists the stratigraphic intervals of the basin fill considered in the thermal models on top of crustal and upper mantle units of different lithologies.

Structure and thickness of crustal units (Fig. 7) is based mainly on seismic data by Rabbel et al. (1995), Erlström et al. (1997), DEKORP-BASIN Research Group (1998, 1999), Arlitt et al. (1999), Bayer et al. (1999), Bleibinhaus et al. (1999), Gossler et al. (1999), Wilde-Piórko et al. (2002), and Krawczyk et al. (2002) and supplemented by gravity models (Scheck et al., 1999, 2002; Kuder, 2002; Lassen et al., 2002). However, crustal structure and composition cannot be unambiguously determined.

For example, P-wave velocity (V_p) data from wide-angle seismic survey are available only for the north-eastern part (km 180−500) of the transect (Fig. 7; Bayer et al., 1999; Bleibinhaus et al., 1999). Velocities range from about 5.3−6.0 km s^{-1} and 6.1−6.4 km s^{-1} in the upper crust, to about 6.5−6.7 km s^{-1} in the middle crust and about 6.8−7.2 km s^{-1} in the lower crust. For the area of the CDF (km 400), Bleibinhaus et al. (1999) assume an interruption of the high-velocity lower crust with rocks of lower velocity, whereas Bayer et al. (2002) presume a continuous high-velocity lower crust to km 180.

With regard to V_p data and interpretations of gravity, magnetic, and magneto-telluric surveys, two different basic scenarios of NEGB crust need to be considered (Fig. 8, Table 3). The two scenarios of crustal structure and composition differ in the interpretation of the Pritzwalk gravity anomaly in the central part of the basin and of lower crust observed south of the CDF. *Crustal scenario A* (Fig. 8a) follows for the Pritzwalk area an interpretation by Lassen et al. (2002) and Bayer et al. (2002), assuming that Caledonian crust (polygons 3 and 9) of Avalonia is amalgamated with Baltica crust (polygons 5−7). Thereby, oceanic crust (polygon 4) was overthrusted onto Baltica. In the northern part of the section, the high-velocity Baltica lower crust (polygons 5−7) is not interrupted at the CDF (km 400). *Crustal scenario B* (Fig. 8b) follows for the Pritzwalk area an interpretation by Franke et al. (1996) and a 3-D gravity model by Kuder (2002). The lower crust is here composed of different terrane units (polygons 3, 4, 5, and LC) supposed not related to Baltica. A mafic intrusion (polygon IN) is emplaced in the crust above a thickened lower crust. In addition, scenario B considers at the CDF (km 400) according to Bleibinhaus et al. (1999) a separation of high-velocity lower crust by rocks of lower V_p (polygon 6).

4.1.2 Thermophysical properties of the crust

Selection of thermal properties of the sedimentary formations in the NEGB is based mainly on information on properties of similar rock types from adjacent areas and supplemented by measurements performed as part of this heat-

flow study. Table 3 lists the thermal properties and density values used in this study for the basin fill as well as for the underlying crust and upper mantle units. Rock type and thickness of each crustal unit is derived from seismic information, basically from the V_p distribution using a procedure similar to that used in Balling (1995). In areas without velocity control, gravity models were used to translate density into V_p and rock type for in-situ pressure and temperature using relations of Christensen and Mooney (1995). Thermal conductivity of supra-Permian sedimentary units is based on data by Balling et al. (1981) and Schön (1996) extrapolated to the conditions of the NEGB; of the Upper Permian (Zechstein) by Balling et al. (1981) and Kopietz et al. (1995); and of the Lower Permian (Rotliegend) and the Permo-Carboniferous magmatic rocks by Norden and Förster (2006). Values assigned to deeper crustal units are according to Schön (1996) and Seipold (2001). A correction of λ to in-situ temperature and pressure conditions is made (cf. Table 3).

The A values of the supra-Permian formations and the Permo-Carboniferous volcanic complexes are from Norden and Förster (2006). It is well known that the estimation of the distribution A for crustal units in general is difficult. We use a stepwise variation of this parameter. The values for the different rock types are based mainly on the data compilation by Čermák et al. (1982). The middle and lower crust is assumed generally not to be anomalously rich in radioactive elements.

4.2 Modelling results

Geotherms calculated using the mean q_s of the NEGB and the standard deviation of the mean (77 ± 3 mW m^{-2}), show remarkably different Moho temperatures in three key areas, at the Binz 1/73 location (close to the CDF), the Gap 1/86 location (southern basin margin; south of the Elbe line), and between these two locations (Gs 2/67; see Fig. 3). The different temperatures (Table 4) result from different λ and A distributions associated with different crustal compositions (Table 3, Fig. 8). Mean Moho temperatures range from 740 to 923 °C. Depending on the amount of heat flow generated in the crust, q_m is in the range of 32 – 41 mW m^{-2}.

One-dimensional temperature models indicate different depths to the lithosphere-asthenosphere boundary (LAB). In this study we focus on the thermal lithosphere, which in our thermal models is approximated by a 1300 °C isotherm (cf. Morgan, 1984; Turcotte and Schubert, 2002). The simple 1-D models result in LAB depths between a minimum of 59 km and a maximum of 111 km (Table 4). The observed range of LAB depths is large and shows a regional variability beneath the NEGB that is considered to be unlikely. To further elaborate the thermal system, 2-D numerical modelling is applied.

5. Heat flow and thermal structure of the lithosphere

A series of 2-D lithospheric thermal models is generated, in which the thermal boundary conditions and the conceptual crustal models are varied to investigate the sensitivity of spatial distribution of heat flow and temperature

related to parameter changes. Modelled q_s is compared to our observed q_s from boreholes in the vicinity of the DEKORP-BASIN 9601 line and projected onto the cross section.

We assume the present thermal state of the lithosphere of the NEGB to be in a steady-state condition. The last major thermal event occurred during the late Carboniferous and early Permian about 300 Ma years ago; later thermal events were less significant (cf. section 2). As was shown for the North Sea Basins by integrated thermomechanical modelling (Frederiksen et al., 2001a, b), 100 Ma after a significant thermal event is sufficient for the system to reach a quasi-steady state with only minor thermal contraction and subsidence.

Although thermal perturbations in the lithosphere-asthenosphere system associated with the Alpine orogeny may be present in the North German Basin, the Cenozoic vertical movements seem to be mainly due to lithospheric compression and relaxation (Gemmer et al., 2003) and the thermal components are of secondary order.

5.1 Two-dimensional numerical models

The equation for two-dimensional steady-state heat conduction is given by

$$\frac{\partial}{\partial x}\left(\lambda\frac{\partial T}{\partial x}\right)+\frac{\partial}{\partial z}\left(\lambda\frac{\partial T}{\partial z}\right)=-A\,. \qquad (4)$$

whereby A is the internal heat production and the thermal conductivity (λ) of the rock is assumed to be isotropic. Equation (4) can be solved numerically. Thereby, the temperature distribution T(x, z) within the lithosphere (with (x) the horizontal coordinate and (z) the vertical coordinate) is determined by the temperature-dependent thermal conductivity distribution λ(x, z), the heat production distribution A(x, z), and the appropriate thermal boundary conditions. The heat equation is solved by the numerical finite-element approach using the PDE toolbox of the commercial software MATLAB 6.5. The finite-element mesh size is variable according to the different size of the crustal polygons (Fig. 8). Polygons representing the sedimentary formations have a mesh size of about 200 x 200 m, and those representing the deeper lithosphere have a mesh size of up to 10 x 8 km.

In the modelling, a constant surface temperature of 8 °C is used. The 1300 °C isotherm (base thermal lithosphere) at laterally varying depth forms the lower boundary condition. At the side boundaries of the 2-D models, horizontal temperature gradients are assumed to be zero (no horizontal heat transfer). To exclude any significant influence of the side boundary conditions on the modelling results along the main section, the model was extended by 250 km in NE and SW direction, respectively (not shown in Figs. 7 and 8).

5.1.1 Structure of the lithosphere

The most detailed information on the structure of the lithosphere-asthenosphere system beneath northern Germany and across the Tornquist

Zone into the southern part of the Baltic Shield is available from the teleseismic TOR project ("Teleseismic TOmography Experiment across the TORnquist Zone", cf. Gregersen et al., 2002). The seismological models for northern Germany indicate a thickness of the lithosphere of less than 100 km, but estimates range from about 50 km to up to about 125 km across the area. All models show a marked thickening of the lithosphere towards the Baltic Shield. The lithospheric boundary in the vicinity of the STZ is sharp and steep. In contrast, the thickness of the crust along the section does not vary markedly (Fig. 7). The seismological information forms our background for testing a suite of lithospheric thermal models with base thermal lithosphere at depths between 50 km and 125 km beneath the NEGB increasing to 200 km beneath the Baltic Shield (Fig. 7).

5.1.2 Thermophysical properties of the lithosphere

The thermal properties (Table 3) of the crust are described in section 4.1.2. The parameters assigned to mantle lithosphere, for which a peridotite composition is used, are from Rudnick and Fountain (1995) and Förster and Förster (2000). For the thermal conductivity, temperature and pressure dependence is included and at temperature >600 °C a component of heat transfer by radiation is also included.

5.2 Modelling results

Figure 9 shows the 2-D thermal modelling results for both crustal scenarios A and B (Fig. 8, section 4.1.2) based on our preferred base thermal lithosphere scenario at a depth of 75 km beneath the NEGB (LAB-75-km model). In the area of the NEGB (km 100−350), modelled q_s of about 75 mW m^{-2} is in good agreement with the observed q_s; departures are within the uncertainty of q_s (section 3). Variations in modelled q_s from the different LAB boundary positions are shown in Figures 10 and 11 and discussed later in this section.

Observed high q_s in the Sw 2/64 borehole (91 mW m^{-2}, Table 1 and Fig. 9) is clearly above the modelled trend and seems to be affected by local conditions not accounted for. Modelled erratic q_s at the basin margins with local amplitudes of 5-10 mW m^{-2} (minima and maxima at km 25, 90, 100, 400, and 460) are the result of thermal refraction between high-thermal-conductivity basement and the sedimentary basin fill of lower conductivity.

Superimposed on the general heat flow trend are modelled local q_s and q_m anomalies caused by local changes in crustal composition. For example, in the Pritzwalk area, mafic intrusive rocks (scenario B) of low A (0.4 µW m^{-3}) and low λ (2.0 W^{-1} m^{-1} K^{-1}) cause a decrease in q_s by >10 mW m^{-2} and an increase in q_m by about 5−10 mW m^{-2} (Fig. 9A, B). At the CDF to the north, changes in crustal composition by replacing mafic granulites (0.1 µW m^{-3}, 2.2 $W^{-1}m^{-1}K^{-1}$; Table 3) by felsic granulites (scenario B; 0.8 µW m^{-3}, 2.7 $W^{-1}m^{-1}K^{-1}$) result in a local decrease in q_m of close to 5 mW m^{-2}. With respect to temperature, the crustal scenarios A and B differ by 40−60 °C in the upper

and lower crust in the Pritzwalk area and by about 30 °C in the lower crust at the CDF (Fig. 9C). The overthrusted oceanic crust (scenario A) at Pritzwalk causes a local perturbation of the heat-flow pattern in the lower crust (illustrated by the 35 and 40 mW m^{-2} isolines, Fig. 9D).

The sensitivity of different depth positions of the LAB beneath the NEGB on heat flow and temperature structure is shown in Figs. 10 and 11. At the northern end of the section (km 400−500), where LAB depth is not varied, all models show q_s of about 50−60 mW m^{-2}, in agreement with the general level of observations in adjacent areas of southern Sweden (Balling, 1995). Within a few kilometres to the south, modelled q_s increases markedly at around the CDF. This sudden increase is caused mainly by a thicker middle crust, and hence higher A (see Fig. 8 and Table 3: polygons 13 and 15) and by the generally thinned lithosphere. Farther to the south, q_s remains high, depending on the LAB scenario, and increases again from km 100−0 in the Variscan belt (Figs. 10 and 11). This increase, which again is different depending of the LAB scenario used, is a reflection of a thick upper and middle crust of granitic to granodioritic composition with moderate to high A values (Table 3) and the typical lower crust composed of mafic granulite (low A) missing (Fig. 8). The general plateau-shaped configuration of q_s in the NEGB (km 100−330) exposes a minor depression between km 100−250 associated with different crustal composition compared to the bordering areas. This depression gets wider in models in which the LAB is deep (Fig. 11 A1).

The different LAB depth scenarios (50, 75, 100 and 125 km) employed in the modelling (other basic parameters being unchanged) result in modelled q_s of about 85, 75, 70 and 65 mW m^{-2}, respectively (Figs. 9, 10 and 11). The variable LAB depth model (about 90-125 km) of Plomerova et al. (2002) shows q_s very similar to the LAB-100-km model. Short wavelength variations on a horizontal length scale of some 100-150 km may not be significantly reflected in surface heat flow.

The lithospheric models also show the contribution to heat flow from the mantle, q_m along the section. Similar to q_s, q_m also varies depending on the LAB position (Figs. 9, 10 and 11). For the preferred LAB-75-km model, q_m is < 30 mW m^{-2} at the northern end of the section and increases to between 35 and 40 mW m^{-2} beneath the NEGB. Because, within certain limits, there is a trade off between A in the crust and q_m for a given q_s, q_m can be lowered if A is increased. This is proposed for the southern end of the section, where q_m of 30 mW m^{-2} is associated with a higher A in the crust that differs from the crust beneath the NEGB. In general, an increase in LAB depths causes a decrease of q_m. For example, in the deep LAB-125-km model, q_m is reduced to less than 30 mW m^{-2} (Fig. 11A1).

The application of different scenarios of LAB depths provides temperature envelops at the Moho. In the northern part of the basin at about the CDF, the Moho temperature is around 600 °C. Beneath the centre and southern margin of the NEGB, the preferred LAB-75-km model has Moho temperatures of

about 800 °C, with 900-1000 °C temperatures to the south beneath the Hartz Mountains. Variation of the level of LAB depths by 25 km results in a change of Moho temperatures by between 75 and 200 °C. The LAB-50-km model shows very high Moho temperatures, about 1000 °C beneath the basin (Fig. 10A2).

6. Discussion

This paper presents for the first time for the NEGB, q_s values together with the input data upon which the determinations were based. This is an advantage compared to previous values (Hurtig and Rockel, 1992) used for a recent heat-flow map of Europe (Hurter and Haenel, 2002). The q_s presented in this paper by 13 new determinations for the NEGB (range 68−91 mW m^{-2}; mean 77 mW m^{-2}) supports the results by Vosteen et al. (2004), who conducted inverse thermal modelling based on thermal properties of the sedimentary cover and the Permian-Carboniferous volcanic rocks. In their study, heat flow was modelled at 6 km depth from an a priori heat flow along the DEKORP-BASIN 9601 line and yields maximum values of about 60−65 mW m^{-2}, depending on the scenarios used. Although their fit of modelled temperature to measured temperature profiles is somewhat ambiguous and in some areas not possible for depth >2 km, it is supposed that the a posteriori heat flow at the depth of the pre-Permian is valid. If heat production for a 6-km interval is taken into account, corresponding to about 11 mW m^{-2} (MV area, Fig. 10 in Norden and Förster, 2006), results on q_s are compatible.

The thermal models show that thermal refraction due to contrasts in λ between basement and the sedimentary basin fill (see also Balling, 1995; Hansen and Nielsen, 2002) results in q_s deviating from the general trend by 5-10 mW m^{-2} at the basin margins. Also significant are effects on q_s of differences in crustal structure and composition. However, the largest of such potential compositional anomalies in the Pritzwalk area unfortunately is devoid of q_s observations. Thus it cannot be verified by the present data whether a thick complex of mafic rock emplaced at mid-crustal level above a thick lower crust (Franke et al. 1996; Kuder, 2002) has to be preferred over the other scenario that favours the amalgamation of Caledonian Avalonia crust to Baltica crust and the overthrusting of oceanic crustal material onto Baltica (Lassen et al., 2002; Bayer et al., 2002).

The high average q_s in the NEGB of 77 mW m^{-2} correlates with the heat flow of provinces younger than 250 Ma (Sclater et al., 1980; Sclater et al., 1981) and is in contrast to values from older, tectonically stable provinces (50 mW m^{-2}). The range of q_s in the NEGB is similar to observations made farther east, in the western part of PB (Fig. 1; 60−90 mW m^{-2}, Majorowicz et al., 2003), which also originated in post-Variscan time. The q_s values of these basins are in contrast to those from the NWGB, where large subareas of lower values (50–70 mW m^{-2}, Hurter and Haenel, 2002) exist. Along the EGT-line (Fig. 2), q_s of 60–68 mW m^{-2} was modelled (Balling,1995).

Removal of the crustal A from the observed q_s values provides by means of q_m insight in the deeper heat budget and in thermal anomalies associated with variations in the thickness of the thermal lithosphere. The q_m inferred for the NEGB from the conceptual structural model and from 2-D lithosphere modelling (35−40 mW m^{-2}, Fig. 9A) is similar to q_m obtained in the adjacent areas north of the CDF (38 mW m^{-2}; Balling, 1995) and similar to values inferred for the PB in the Variscan belt south of the TTZ in Poland (35−40 mW m^{-2}, Majorowicz et al., 2003). The level of q_m obtained for the NEGB is significantly higher than the value of 25 mW m^{-2} applied by Bayer et al. (1997) and Ondrak et al. (1998). The latter q_m value is typical for areas bordering the NEGB to the north and northeast, towards the Baltic Shield and the stable East European Craton (20−30 mW m^{-2}; Čermák, 1993; Balling, 1995). The Baltic Shield itself exposes maximum lithosphere thicknesses (160-240 km, Kukkonen and Peltonen, 1999) in the Archaean craton area, corresponding to a q_m in the range of 12 $\pm$ 5 mW m^{-2}. The Proterzoic areas of the shield are characterized by q_m of 19 $\pm$ 6 mW m^{-2} (Kukkonen and Jõeleht, 1996).

In the NEGB models, an increase of crustal A on the expense of q_m to accommodate the high q_s seems unjustified. Crustal heat flow is relatively high (36-45 mW m^{-2}, Table 4) and at the upper limit of estimates for bulk continental crust (24−38 mW m^{-2}; Rudnick et al., 1998). This crustal heat flow is similar to the situation in the southern part of the PB (37 mW m^{-2}; Majorowicz et al., 2003). For comparison, the respective value for the thicker crust in the Baltic Shield (northern part of the EGT) is about 30 mW m^{-2}

(Balling, 1995), for Baltica crust north of NEGB (this study) about 23 mW m^{-2} and for the East European Craton in Poland about 20 mW m^{-2} (Majorowicz et al., 2003). We therefore consider the high q_m values in the NEGB as realistic and to correlate with a thermal lithosphere that is significantly reduced in thickness compared to areas to the north.

On a regional scale, the European continental lithosphere north of the Alps is characterized by a strong variation in structure and thickness (e.g. Blundell, 1999). Whereas the crust of the Baltic Shield is ca. 40–50 km thick and laterally relatively uniform in physical properties, the Caledonian/Variscan crust is uniformly about 30 km thick and structurally highly variable. No crustal or lithospheric roots remain to mark the Caledonian and Variscan orogens. Lithospheric thickness changes from 150 to >200 km beneath most of Fennoscandia to values around 100 km along the TTZ, in northern Germany. This value is corroborated also for the area east of the NEGB in Poland (Majorowicz et al., 2003). The major transition of lithospheric thickness from the NEGB towards Fennoscandia is well reflected in q_s.

Narrow heat flow transitions from high heat flow to low heat flow as observed north of the NEGB across the STZ are observed along most of the Tornquist Zone from the Black Sea to the North Sea. This thermal boundary is also a marked boundary in terms of large changes in lithospheric thickness (e.g. Zielhuis and Nolet, 1994b; Artemieva et al., 2006).

Our preferred model of a 75-km-thick thermal lithosphere is corroborated by seismological results. From broad-band TOR- data and fundamental Rayleigh-wave analysis Cotte et al. (2002) modelled for northern Germany the top of the low S-velocity asthenosphere (LAB) at a depth of 100 ± 20 km regionally and for two local subarrays at 50 ± 10 km and 75 ± 25 km. High resolution travel-time tomography on the entire TOR data set, using different inverse modelling procedures (Arlitt, 1999; Shomali et al.,2002, 2006; Voss et al., 2006) also show thin lithosphere beneath northern Germany (south of CDF, Fig. 1). Plomerová et al. (2002), also using TOR-data, model lithosphere thickness along the TOR array from relative P-wave travel- time residuals and empirical relations to vary in northern Germany between about 50 km (northwest) and about 125 km (southeast). Although crustal corrections were applied, remaining residuals may not in a simple way reflect lithospheric thickness variations, and reported variations may be overestimated. In addition, a LAB at shallow depths of 50 km cannot be readily assumed for the NEGB from a thermal point of view. Those conditions, known from the Basin and Range Province in North America (Goes and van der Lee, 2002), produce at a regional scale q_s values in the order of 80-100 mW m^{-2} (Blackwell and Richards, 2004), values that are not observed in the NEGB. The high q_s in the Basin and Range Province is related to a temperature increase in the deeper mantle compared to surrounding continental mantle, that can explain the over 2 km of mantle-induced topography in this area (Goes and van der Lee, 2002). Such conditions are very different from those of the NEGB of low topography (Reicherter et al., 2005).

Significant lithospheric thickness variations across northern Germany including the NEGB as suggested by Plomerová et al. (2002) (Fig. 11B) are not resolved by our thermal models and are in some contrast to other modelling results of the TOR data. It is also not resolved whether a quasi plateau-shape LAB holds true for the Variscan crust farther south of the NEGB, in areas not affected by young volcanism. Babuška and Plomerová (1992) introduced for the Saxothuringian of Europe lithospheric thicknesses on the order of 90−120 km; Heuer (2006) reports from teleseismic receiver-function analysis a LAB at 80−90 km beneath the Saxothuringian and the northern Teplá-Barrandian unit.

The temperature pattern of the European lithospheric mantle at 100 km depth provided by Goes et al. (2000), based on inversion of the seismic velocity models by Bijwaard et al. (1998) and Marquering and Snieder (1996), shows values for the NEGB on the order of 1300−1400 °C from inverted S-wave data and <1100 °C from inverted P-wave data. Only the temperatures inferred from S-velocity is supported by our thermal models. The P-wave data suggest a thermal LAB (1300 °C) at depth >100 km.

The model of the 75-km-thick thermal lithosphere beneath the NEGB shows Moho temperatures that increase from the northern part of the basin (about 600 °C at the CDF) progressively to the south (800 °C beneath the centre and southern margin of the NEGB, 900−1000 °C beneath the Harz Mountains).

The 1-D geotherm Moho temperatures (based on a q_s of 77 mW m^{-2}, Table 4) are somewhat higher than in the 2-D model (740 °C close to the CDF, 920 °C at the basin centre and lower at the southern margin (about 855 °C). Our 2-D models are preferred over the 1-D models due to the more accurate modelling of laterally varying crustal thermal properties and as well as of the laterally varying lower boundary condition. The temperatures in the centre of the NEGB correspond to values modelled for the PB (profile P1, Majorowicz et al., 2003).

Temperature of < 600 °C modelled for the uppermost lithospheric mantle to the north of the NEGB would translate according to the Black and Braile (1982) relations into upper mantle seismic V_p values > 8.1 km s^{-1}. This is in agreement with the seismic velocities obtained by Bleibinhaus et al. (1999) in the northern NEGB and in the Rügen area (Fig. 7) thus supporting our thermal model. Unfortunately, the southern part of the NEGB and adjacent areas to the south lack data on crustal and upper mantle seismic velocities. From our temperature models, V_p < 6.9−7.0 km s^{-1} is to be expected for the lower crust and V_p < 8.0 km s^{-1} for the upper mantle. Low upper mantle V_p of 7.8−8.0 km s^{-1} was shown for the EGT-profile farther west in the transition zone to the Variscan belt (Aichroth et al., 1992; Thybo, 1997) corresponding to temperatures between 750°C and 1000°C (Black and Braile, 1982). This corresponds to temperatures modelled for the central and southern part of the NEGB.

The LAB-75-km thermal model (and also the LAB-100-km model) shows for the southern margin of the NEGB a transition from lower q_s (km 100−250) to an area of higher q_s (km 0−100). This transition in the models is sharp and significant and entirely associated with a crust of different composition and which thickens to the south. This thermal transition is likely to have rheological implications. Thus Scheck et al. (2002) assume for the area of the Elbe Fault System, which borders the NEGB to the south at about km 100 in profile section (Figs. 7 and 8) a weak, stress-sensitive zone in the lower crust as the reason for the high mobility of the area and repeated strain localisation. This zone received the most intensive deformation during late Cretaceous – early Cenozoic times, whereas the central part of the basin remained more or less stable during recent basin evolution (Marotta et al., 2000; Gemmer et al., 2003).

The combined thermal information from this study and the seismological information on the lithosphere-asthenosphere system, mainly from the TOR project, consistently indicate the existence of a rather thin lithosphere (75–100 km thick) beneath large parts of northern Germany including the Northeast German Basin. The warm nature of the lithosphere is corroborated by the aseismic behaviour of the NEGB as shown by Marotta et al. (2002).

Since the last major thermal event dates back to the late Carboniferous early Permian some 300 Ma ago (section 2) it needs to be studied whether a later thermal process is needed to maintain or generate a relatively thin lithosphere

beneath the NEGB. There has been suggestions that the large contrasts in P- and S-wave velocities in the upper mantle and the steep LAB boundary along the STZ could not be of purely thermal origin but additional compositional effect should be present (e.g. Shomali et al., 2006). This problem has recently been addressed by Hieronymus et al. (2007), who find that the large differences in seismic velocities are to a large extent caused by temperature differences and that compositional difference has relatively minor effect. They argue for a dynamic mantle with some convective transfer of heat in addition to pure conduction to maintain a large contrast for a very long time. A thin lithosphere beneath northern Germany may have been formed and maintained by a combination of different processes that are not included in the present models. However, we believe that the steady-state thermal models presented can be applied to the NEGB and that our preferred lithospheric model (Fig. 9) contains main thermal characteristics in terms of temperature distribution in the crust and uppermost mantle consistent with the thickness of the thermal lithosphere. The data and models of this study should provide a good thermal background for integrated modelling and interpretation of the geodynamics of this basin.

Acknowledgements

The EEG Erdgas Erdöl GmbH (Berlin) and the EWE AG (Oldenburg) are thanked for providing parts of the industrial borehole data. The geological surveys: Landesamt für Bergbau, Geologie und Rohstoffe Brandenburg

(Cottbus/Kleinmachnow); Landesamt für Umwelt, Naturschutz und Geologie Mecklenburg-Vorpommern (Schwerin); and Geologisches Landesamt Sachsen-Anhalt (Halle) are acknowledged for the supply of borehole information and for the support of the core sampling. D. Stromeyer is thanked for his help to implement the thermal crustal model to the Matlab environment. The work benefited from discussions with H.-J. Götze (Kiel) and R. Kind (Potsdam).

References

Aichroth, B., Prodehl, C., Thybo, H., 1992. Crustal structure along the central segment of the EGT from seismic refraction studies. Tectonophysics 207, 43—64.

Arlitt, R., Kissling, E., Ansorge, J., Group, T. W., 1999. Three-dimensional crustal structure beneath the TOR array and effects on teleseismic wavefronts. Tectonophysics 314, 309—319.

Arlitt, R., 1999. Teleseismic body wave tomography across the Trans-European Suture Zone between Sweden and Denmark. Ph.D. thesis, ETH Zurich.

Artemieva, I.; Thybo, H.; Kaban, M., 2006. Deep Europe today: geophysical synthesis of the upper mantle structure and lithospheric processes over 3.5Ga. In: Gee, D. G.; Stephenson, R. A. (Eds.), European Lithosphere Dynamics, Geological Society, London, 11—41.

Babuška, V., Plomerová, J., 1992. The lithosphere in central Europe – Seismological and petrological aspects. Tectonophysics 207, 141—163.

Balling, N., Kristiansen, J. I., Breiner, N., Poulsen, K. D., Rasmussen, R., Saxov, S., 1981. Geothermal measurements and subsurface temperature modelling in Denmark. Tech. Rep. Geoskrifter No.16, Department of Geology, Aarhus University, ISSN 0105-824X.

Balling, N., 1995. Heat flow and thermal structure of the lithosphere across the Baltic Shield and northern Tornquist Zone. Tectonophysics 244, 13—50.

Bayer, U., Scheck, M., Koehler, M., 1997. Modelling of the 3D thermal field in the northeast German Basin. Geol. Rundschau 86, 241—251.

Bayer, U., Scheck, M., Rabbel, W., Krawczyk, C., Götze, H.-J., Stiller, M., Beilecke, T., Marotta, A.-M., Barrio-Alvers, L., Kuder, J., 1999. An integrated study of the NE German Basin. Tectonophysics 314, 285—307.

Bayer, U., Grad, M., Pharaoh, T., Thybo, H., Guterch, A., Banka, D., Lamarche, J., Lassen, A., Lewerenz, B., Scheck, M., Marotta, A.-M., 2002. The southern margin of the East European Craton: new results from seismic sounding and potential fields between the North Sea and Poland. Tectonophysics 360, 301—314.

Beck, A., 1977. Climatically perturbed temperature gradients and their effect on regional and continental heat flow means. Tectonophysics 41, 17—39.

Benek, R., Eckhardt, F.-J., Huebscher, H.-D., Korich, D., Kramer, W., Marx, J., Negendank, J. F., Tobschall, H. J., 1995. Massenbilanzen und Quantifizierung der stofflich-genetischen Entwicklung permokarboner Magmatite der Norddeutschen Senke als Beitrag zur Modellierung spätorogener Becken. Final report DFG project To53/14-2, GeoForschungsZentrum Potsdam.

Benek, R., Kramer, W., McCann, T., Scheck, M., Negendank, J., Korich, D., Huebscher, H.-D., Bayer, U., 1996. Permo-carboniferous magmatism of the Northeast German Basin. Tectonophysics 266, 379—404.

Bijwaard, H., Spakman, W., Engdahl, E.R., 1998. Closing the gap between regional and global travel time tomography. Journal of Geophysical Research 103; 30,055—30,078.

Black, P., Braile, L., 1982. Pn velocity and cooling of the continental lithosphere. J. Geophys. Res. 87, 10557—10568.

Blackwell, D. D., Spafford, R. E., 1987. Experimental methods in continental heat flow. In: Sammis, C. G., Henyey, T. L. (Eds.), Methods of Experimental Physics, v. 24 Geophysics, Part B Field Measurements. Academic Press, Orlando, 189—226.

Blackwell, D. D., Richards, M., 2004. Geothermal Map of North America. American Assoc. Petroleum Geologist (AAPG), 1 sheet, scale 1:6,500,000.

Blundell, D.J., 1999. The legacy of the European Geotraverse. Tectonophysics 314, 7—16.

Bleibinhaus, F., Beilecke, T., Bram, K., Gebrande, H., 1999. A seismic velocity model for the SW Baltic Sea derived from BASIN'96 refraction seismic data. Tectonophysics 314, 269—283.

Čermák, V., 1993. Lithospheric thermal regimes in Europe. Physics of the Earth and Planetary Interiors 79, 179—193.

Čermák, V., Huckenholz, H.-G., Rybach, L., Schmid, R., Schopper, J. R., Schuch, M., Stöffler, D., Wohlenberg, J., 1982. Physical properties of rocks. In: Angenheister, G. (Ed.), Landolt-Börnstein. Vol. 1a. Springer, Heidelberg, 1—373.

Christensen, N. I., Mooney, W. D., 1995. Seismic velocity structure and composition of the continental crust: A global view. Journal of Geophysical Research 100, 9761—9788.

Cloetingh, S., Ziegler, P.A., Beekman, F., Andriessen, P.A.M., Matenco, L., Bada, G., Carcia-Castellanos, D., Hardebol, N., Dèzes, P., Sokoutis, D., 2005. Lithospheric memory, state of stress and rheology: neotectonic controls on Europe's intraplate continental topography. Quaternary Science Reviews 24, 241—304.

Cotte, N., Pedersen, H., TOR Working Group, 2002. Sharp contrast in lithospheric structure across the Sorgenfrei-Tornquist Zone as inferred by Rayleigh wave analysis of TOR1 project data. Tectonophysics 360, 75—88.

DEKORP-BASIN Research Group, 1998. Survey provides seismic insights into an old suture zone. EOS 79 (12), 151, 159.

DEKORP-BASIN Research Group, 1999. Deep crustal structure of the Northeast German Basin: New DEKORP-BASIN'96 deep-profiling results. Geology 27 (1), 55—58.

Erlström, M., Thomas, S., Deeks, N., Sivhed, U., 1997. Structure and tectonic evolution of the Tornquist Zone and adjacent sedimentary basins in Scania and the southern Baltic Sea area. Tectonophysics 271, 191—215.

Förster, A., 2001, Analysis of temperature data in the Northeast German Basin: continuous logs versus bottom-hole temperatures. Petroleum Geoscience 7, 241—254.

Förster, A., Förster, H.-J., 2000. Crustal composition and mantle heat flow: implications from surface heat flow and radiogenic heat production in the Variscan Erzgebirge (Germany). Journal of Geophysical Research 105 (B12), 27,917—27,938.

Franke, D., Hoffmann, N., Lindert, W., 1996. The Variscan deformation front in East Germany. Part 2: Tectonic interpretation. Z. angew. Geol. 42, 44—56.

Frederiksen, S., Nielsen, S.B., Balling, N., 2001. A numerical dynamic model for the Norwegian-Danish Basin. Tectonophysics 343. 165—183.

Frederiksen, S., Nielsen, S.B., Balling, N., 2001: Post Permian evolution of the Central North Sea: a numerical model. Tectonophysics 343. 185—203.

Friberg, L. J., Poelchau, H., Krooss, B., Littke, R., 2000. 3D-modelling of the thermal history and simulation of methane and nitrogen migration

along the Northeast German seismic DEKORP profie 9601. Journal of Geochemical Exploration 69-70, 263—267.

Friberg, L. J., 2001. Untersuchungen zur Temperatur- und Absenkungsgeschichte sowie zur Bildung und Migration von Methan und molekularem Stickstoff im Nordostdeutschen Becken. Ph.D. thesis, RWTH Aachen, reports of the Forschungszentrums Jülich Nr. 3914.

Gemmer, L., Nielsen, S. B., Bayer, U., 2003. Late Cretaceous-Cenozoic evolution of the North German Basin – results from 3-D geodynamic modelling. Tectonophysics 373, 39—54.

Glennie, K. W., 1998. Lower Permian - Rotliegend. In: Glennie, K. W. (Ed.), Petroleum Geology of the North Sea - Basic Concepts and Recent Advances. Blackwell Science, London, pp. 137—173.

Goes, S., Govers, R., Vacher, P., 2000. Shallow mantle temperatures under Europe from P and S wave tomography. Journal of Geophysical Research 105; 11,153—11,169.

Goes, S., van der Lee, S., 2002. Thermal structure of the North American uppermost mantle inferred from seismic tomography. Journal of Geophysical Research 107; B3, 2050, 10-1029/2000JB000049.

Gossler, J., Kind, R., Sobolev, S. V., Kämpf, H., Wylegalla, K., Stiller, M., TOR Working Group, 1999. Major crustal features between the Harz Mountains and the Baltic Shield derived from receiver functions. Tectonophysics 314, 321—333.

Gregersen, S., Voss, P., TOR Working Group, 2002. Summary of project TOR: delineation of a stepwise, sharp, deep lithosphere transition across Germany - Denmark - Sweden. Tectonophysics 360, 61—73.

Hansen, D., Nielsen, S., 2002. Does thermal weakening explain basin inversion? stochastic modelling of the thermal structure beneath sedimentary basins. Earth and Planetary Science Letters 198, 113—127.

Heuer, B., 2006. Lithospheric and upper mantle structure beneath the western Bohemian Massif obtained from teleseismic P and S receiver functions. Scientific Technical Report STR06/12, GeoForschungsZentrum Potsdam, Potsdam, 149 p.

Hoffmann, N., Jödicke, H., Fluche, B., Jording, A., Müller, W., 1998. Modellvorstellungen zur Verbreitung potentieller präwestfälischer Erdgas-Muttergesteine in Norddeutschland - Ergebnisse neuer magnetotellurischer Messungen. Z. angew. Geol. 44, 140—158.

Hoth, K., Rusbült, J., Zagora, K., Beer, H., Hartmann, O., 1993: Die tiefen Bohrungen im Zentralabschnitt der mitteleuropäischen Senke – Dokumentation für den Zeitabschnitt 1962-1990, Schriftenreihe für Geowissenschaften, 2, 145.

Hurter, S., 2002. Logging Interpretation in Groß Schönebeck: well deviation, calliper, pressure, temperature, mud resistivity. In: Huenges, E., Hurter, S. (Eds.), In-situ Geothermielabor Groß Schönebeck 2000/2001, Scientific Technical Report STR02/14, GeoForschungsZentrum Potsdam, 87—107.

Hurter, S., Haenel, R. (Eds.), 2002. Atlas of geothermal resources in Europe. Office for Official Publications of the European Communities, Luxemburg, p. 93, 89 plates.

Hurtig, E., Rockel, W., 1992. Federal Republic of Germany, eastern federal states. In: Hurtig, E., Čermak, V., Haenel, R., Zui, V. (Eds.), Geothermal Atlas of Europe. Hermann Haak Verlagsgesellschaft mbH, Gotha, pp. 38—40, 115—118.

Karnkowski, P.H., 1999. Origin and evolution of the Polish Rotliegend Basin. Polish Geological Institute Special Papers 3, Warszawa, Poland, p.93.

Katzung, G., Ehmke, G., 1993. Das Prätertiär in Ostdeutschland. Verlag Sven von Loga, Cologne, Germany, p. 139.

Kopietz, J., Greinwald, S., Bochem, M., Mors, K., Czora, C., Koß, G., 1995. Untersuchungen thermophysikalischer und elektrischer Eigenschaften von Salzgesteinen. Final report 0114283, Bundesanstalt für Geowissenschaften und Rohstoffe.

Kossow, D., Krawczyk, C., McCann, T., Strecker, M., Negendank, J. F. W., 2000. Style and evolution of salt pillows and related structures in the northern part of the Northeast German Basin. International Journal of Earth Sciences 89, 652—664.

Kossow, D., Krawczyk, C., 2002. Structure and quantification of processes controlling the evolution of the inverted NE-German Basin. Marine and Petroleum Geology 19, 601—618.

Krawczyk, C., Stiller, M., DEKORP-BASIN Research Group, 1999. Reflection seismic constraints on Paleozoic crustal structure and Moho beneath the NE German Basin. Tectonophysics 314, 241—253.

Krawczyk, C., Eilts, F., Lassen, A., Thybo, H., 2002. Seismic evidence of Caledonian deformed crust and uppermost mantle structures in the northern part of the Trans-Euorpean Suture Zone, SW Baltica Sea. Tectonophysics 360, 215—244.

Kuder, J., 2002. 3D Schwerefeldmodellierung zur Erfassung des tiefen Untergrundes im Nordost-Deutschen Becken. PhD thesis, Freie Universität Berlin.

Kukkonen, I. T., Jõeleht, A., 1996. Geothermal modelling of the lithosphere in the central Baltic Shield and its southern slope. Tectonophysics 255, 25—45.

Kukkonen, I. T., Jõeleht, A., 2003. Weichselian temperatures from geothermal heat flow data. Journal of Geophysical Research B: Solid Earth, 108(3), 9—11.

Kukkonen, I. T., Peltonen, P., 1999. Xenolith-controlled geotherm for the central Fennoscandian Shield: implications for lithosphere-asthenosphere relations. Tectonophysics 304, 301—315.

Lassen, A., Bayer, U., Scheck, M., April 2002. Deep structure of the Eastern North German Basin; possible scenarios of formation modelled and discussed on the basis of seismic and potential field data. In: XXVII General Assembly of the European Geophysical Society. Vol. 4. EGS, Nice, France.

Lokhorst, A., 1998. NW European gas atlas [CD-ROM]. Nederlands Inst. voor Toegepaste Geowetenschappen TNO, Haarlem.

Lotz, B., 2004. Neubewertung des rezenten Wärmestroms im Nordostdeutschen Becken. Scientific Technical Report STR 04/04, GeoForschungszentrum Potsdam.

Majorowicz, J., Čermák, V., Šafanda, J., Krzywiec, P., Wróblewska, M., Guterch, A., Grad, M., 2003. Heat flow models across the Trans-European Suture Zone in the area of the POLONAISE'97 seismic experiment. Physics and Chemistry of the Earth 28, 375—391.

Majorowicz, J., 2004. Thermal lithosphere across the Trans-European Suture Zone in Poland. Geological Quarterly 48 (1), 1—14.

Marotta, A. M., Bayer, U., Thybo, H., 2000. The legacy of the NE German Basin - reactivation by compressional buckling. Terra Nova 12, 132—140.

Marotta, A.M., Bayer, U., Thybo, H., Scheck, M., 2002. Origin of the regional stress in the North German basin: results from numerical modelling. Tectonophysics 360, 245—264.

Marquering, H. Snieder, R., 1996. Shear-wave velocity structure beneath Europe, the northeastern Atlantic and western Asia from waveform inversions including surface-wave mode coupling. Geophysical Journal International 124, 283—304.

Meissner, R., Sadowiak, P., Thomas, S. A., BABEL Working Group, 1994. East Avalonia, the third partner in the Caledonian collision: evidence

from deep seismic reflection data. Geologische Rundschau 83, 186—196.

Morgan, P., 1984. The thermal structure and thermal evolution of the continental lithosphere. In: H.N. Pollack and V.R. Murthy (Editors), Structure and Evolution of the Continental Lithosphere. Phys. Chem. Earth, 15: 107—193.

Norden, B., Förster, A., 2006. Thermal conductivity and radiogenic heat production of sedimentary and magmatic rocks in the Northeast German Basin, AAPG Bulletin, 90 (6), 939—962.

Ondrak, R., Wenderoth, F., Scheck, M., Bayer, U., 1998. Integrated geothermal modelling on different scales in the Northeast German Basin. Geologische Rundschau 87 (1), 32—42.

Pharaoh, T., 1999. Palaeozoic terranes and their lithospheric boundaries within the Trans-European Suture Zone (TESZ): a review. Tectonophysics 314, 17—41.

Plomerová, J., Babuška, V., Vecsey, L., Kouba, D., TOR Working Group, 2002. Seismic anisotropy of the lithosphere around the Trans European Suture Zone (TESZ) based on teleseismic body-wave data of the TOR experiment. Tectonophysics 360, 89—114.

Pollack, H. N., Huang, S., 2000. Climate reconstruction from subsurface temperatures. Annual Review of Earth and Planetary Sciences 28, 339—365.

Powell, W. G., Chapman, D. S., Balling, N., Beck, A. E., 1988. Continental heat-flow density. In: Haenel, R., Rybach, L., Stegena, L. (eds.),

Handbook of Terrestrial Heat-flow Density Determination, 174—213, Kluwer, Dordrecht, Holland.

Rabbel, W., Förste, K., Schulze, A., Bittner, R., Reichert, J., 1995. A high velocity layer in the lower crust of the North German Basin. Terra Nova 7, 327—337.

Reicherter, K., Kaiser, A., Stackebrandt, W., 2005. The post-glacial landscape evolution of the North German Basin: morphology, neotectonics and crustal deformation. International Journal of Earth Sciences 94, 1083—1093.

Rudnick, R. L., Fountain, D. M., 1995. Nature and composition of the continental crust: a lower crustal perspective. Reviews of Geophysics 33 (3), 267—309.

Rudnick, R. L., McDonough, W. F., O'Connell, R. J., 1998. Thermal structure, thickness and composition of continental lithosphere. Chemical Geology 145, 395—411.

Scheck, M., 1997. Dreidimensionale Strukturmodellierung des Nordostdeutschen Beckens unter Einbeziehung von Krustenmodellen. Scientific Technical Report STR 97/10, GeoForschungsZentrum Potsdam.

Scheck, M., Bayer, U., 1999. Evolution of the Northeast German Basin – inferences from a 3D structural model and subsidence analysis. Tectonophysics 313, 145—169.

Scheck, M., Barrio-Alvers, L., Bayer, U., Götze, H.-J., 1999. Density structure of the Northeast German Basin: 3D Modelling along the DEKORP line BASIN96. Phys. Chem. Earth (A) 24 (3), 221—230.

Scheck, M., Bayer, U., Otto, V., Lamarche, J., Banka, D., Pharaoh, T., 2002. The Elbe Fault System in North Central Europe - a basement controlled zone of crustal weakness. Tectonophysics 360, 381—299.

Scheck-Wenderoth, M., Lamarche, J., 2005. Crustal memory and basin evolution in the Central European Basin System - new insight from a 3D structural model. Tectonophysics 397, 143—165.

Schön, J., 1996. Physical properties of rocks: Fundamentals and principles of petrophysics. In: Helbig, K., Teitel, S. (Eds.), Handb. Geophy. Explor., Sect. 1. Vol. 18. Pergamon, Oxford, U.K.

Sclater, J. G., Jaupart, C., Galson, D., 1980. The heat flow through the oceanic and continental crust and the heat loss of the Earth. Reviews of Geophysics and Space Physics, 18, 269—311.

Sclater, J. G., Parsons, B., Jaupart, C., 1981. Oceans and continents : similarities and differences in the mechanisms of heat loss. Journal Geophysical Research 86, 11 535—11 552.

Seipold, U., 2001. Der Wärmetransport in kristallinen Gesteinen unter den Bedingungen der kontinentalen Kruste. Scientific Technical Report STR 01/13, GeoForschungsZentrum Potsdam.

Sekiguchi, K., 1984. A method for determining terrestrial heat flow in oil basinal areas, Tectonophysics 103, 67—79.

Shomali, Z. H., Roberts, R. G., and the TOR Working Group, 2002. Non-linear body wave teleseismic tomography along the TOR array. Geophys. J. Int., 148, 562—574.

Shomali, Z. H., Roberts, R. G., Pedersen, L. B. and the TOR Working Group, 2006. Lithospheric structure of the Tornquist Zone resolved by nonlinear P and S teleseismic tomography along the TOR array. Tectonophysics 416, 133—149.

Somerton, W., 1992. Thermal properties and temperature-related behavior of rock/fluid systems. Elsevier.

Thybo, H., 1997. Geophysical characteristics of the Tornquist Fan area, northwest Trans-European Suture Zone: indication of late Carboniferous to early Permian dextral transtension. Geol. Mag. 5, 567—606.

Turcotte, D. L., Schubert, G., 2002. Geodynamics. Applications of Continuum Physics to Geological Problems. John Wiley & Sons, New York.

van Wees, J.-D., Stephenson, R. A., Ziegler, P. A., Bayer, U., McCann, T., Dadlez, R., Gaupp, R., Narkiewicz, M., Bitzer, F., Scheck, M., 2000. On the origin of the Southern Permian Basin, Central Europe. Marine and Petroleum Geology, 17, 1, 43—59.

Vosteen, H.-D., Rath, V., Schmidt-Mumm, A., Clauser, C., 2004. The thermal regime of the Northeastern-German Basin from 2-D inversion. Tectonophysics 386, 81—95.

Wilde-Piórko, M., Grad, M.,TOR Working Group, 2002. Crustal structure variation from the Precambrian to Palaeozoic platforms in Europe

imaged by the inversion of teleseismic receiver functions - project TOR. Geophys. J. Int. 150, 261—270.

Ziegler, P. A., 1990. Geological Atlas of Western and Central Europe, 2nd Edition. The Hague (Shell).

Ziegler, P. A., Cloetingh, S., van Wees, J. D., 1995. Dynamics of intraplate compressional deformation: the Alpine foreland and other examples. Tectonophysics 252, 7—59.

Zielhuis, A., Nolet, G., 1994a. Shear-wave velocity variations in the upper mantle beneath Central Europe. Geophys. J. Int. 117, 695—715.

Zielhuis, A., Nolet, G., 1994b. Deep seismic expression of an ancient plate boundary in Europe. Science 265, 79—81.

Zoth, G., Haenel, R., 1988. Thermal conductivity. In: Haenel, R., Rybach, L., Stegena, L. (eds.), Handbook of Terrestrial Heat-Flow Density Determination, 449—466, Kluwer Academic Publisher, Dordrecht.

Figures

Figure 1. Study area and main tectonic units of the Southern Permian Basin and adjacent areas (after Bayer et al., 2002; Karnkowski, 1999; Lokhorst, 1998; Pharaoh, 1999; Ziegler, 1990). Abbreviations: CDF Caledonian Deformation Front; DB Danish Basin; EL Elbe Line; MAH Møn Arkona High; NEGB Northeast German Basin; NWGB Northwest German Basin; PB Polish Basin; RFH Rynkøbing Fyn High; STZ Sorgenfrei-Tornquist Zone; TTZ Tornquist-Teisseyre Zone; VDF Variscan Deformation Front. The distribution of Rotliegend (Permian) sedimentary units is gray shaded.

Figure 2. Selected seismic lines across the Trans-European Suture Zone. Lithosphere thermal modelling was performed by Balling (1995) for the EGT and the FENNOLORA profiles and by Majorowicz et al. (2003) and Majorowicz (2004) for the LT-7 profile and other profiles in Poland. The lithosphere thermal modelling presented in this paper is performed along the DEKORP-BASIN9601 profile and its north-eastern extension (PQ2-4 and PQ2-5, together with PQ2-9.1 and DSB-9).

Figure 3. Surface heat-flow density (mW m^{-2}) determined at 13 borehole locations in the NEGB. The depth to top of Permian is shown to delineate the centre and margin of the basin (after Scheck, 1997). Also shown is the main part of the modelled section across the basin and the locations of forward 1-D thermal modelling (thick cross).

Figure 4. Estimated paleoclimatic effects on present-day temperature (A) and temperature gradient (B) for thermal diffusivity values typical for sandstones ($10 \cdot 10^{-7}$ m^2s^{-1}, solid line) and mudstones ($5 \cdot 10^{-7}$ m^2s^{-1}, dashed line). The calculations are based on paleoclimatic data compiled by Zoth and Haenel (1988).

Figure 5. Top view of the Gransee model area. Salt structures are shown in gray and shallow diapirs in dark grey. Also shown are model points (theoretical boreholes A, B, C, D, E, 1 km, 2 km, 3 km, and Margin). The Gs 2/67 borehole location is shown in Figure 3 for geographic reference.

Figure 6. Results from the Gransee salt structure thermal modelling. Depth profiles for temperature (T), temperature gradient (Grad), and vertical heat-flow density (q(z)) are shown. A, effects observed at salt structures 1−6; B, effects observed in the marginal model zone in comparison to conditions at the Gs 2/67 borehole; C, selected observations points near salt structure no. 2 and the margin of the model. For positions of model points see Figure 5.

Figure 7. Structure of the crust based on depth-converted deep seismic reflection profiles DEKORP-BASIN 9601, PQ2-004, PQ2-9.1, DSB-9, and PQ2-005. The line-drawings are from DEKORP-BASIN9601, PQ2-

005, and PQ2-9.1 (after Bayer et al., 1999; 2002). V_p (in km s^{-1}) is from Bleibinhaus et al. (1999) and from Bayer et al. (1999). The different scenarios of thermal LAB depths used as lower boundary constraint in the 2-D thermal modelling (Figs. 9, 10, and 11) are also shown.

Figure 8. Conceptual crustal models used in the thermal modelling. A, crustal scenario A and B, crustal scenario B cf. text. Polygons (marked with encircled numbers and letters) denote units of different lithology inferred from seismic and gravity models (e.g. Lassen, 2002; Kuder, 2002). Thermal parameters are listed in Table 3. Boreholes with heat-flow data adjacent to the section are projected into the line.

Figure 9. Thermal modelling results from our preferred LAB-75-km model (cf. Fig. 7) with crustal scenarios A and B. A, modelled q_s and q_m and comparison to q_s observed in boreholes (dots); B, difference in q_s and q_m from the two crustal scenarios (data from scenario B are subtracted from data of scenario A); C, equivalent temperature difference (°C); D, modelled heat-flow distribution (mW m^{-2}) in the crust and lithospheric mantle (crustal scenario A); E, calculated isotherms (°C) for crustal scenario A. The crust below the sedimentary cover (in white) is gray-shaded. Vertical exaggeration: approximately threefold.

Figure 10. Thermal modelling results from LAB-50-km and LAB-100-km models. Scenario A for the crust. A1 and B1 modelled q_s and q_m in

comparison to observed q_s (dots) projected onto the cross section. A2 and B2 calculated isotherms (°C). The crust below the sedimentary cover (in white) is gray-shaded. Vertical exaggeration: approximately threefold.

Figure 11. Thermal modelling results from LAB-125-km and LAB-Pl models (LAB-Pl after Plomerova et al., 2002; cf. text). Scenario A for the crust. For further details see caption of Figure 10.

Tables

Table 1. New determinations of surface heat-flow (q_s) and associated thermal data for 13 borehole localities (Fig. 3) in the NEGB. See text for explanations.

Table 2. Thermal parameters used in the salt structure thermal modelling.

Table 3. Petrophysical parameters for crust and upper mantle used in the lithospheric thermal modelling. A and B, crustal model senarios as shown in Figure 8.

Table 4. Results of 1-D thermal modelling. Moho temperatures and depth of thermal LAB (1300°C) based on the determined mean heat flow of the

NEGB for three sites (cf. Fig. 3) . Also given is q_m and the heat-flow component from the crust in this 1-D model.

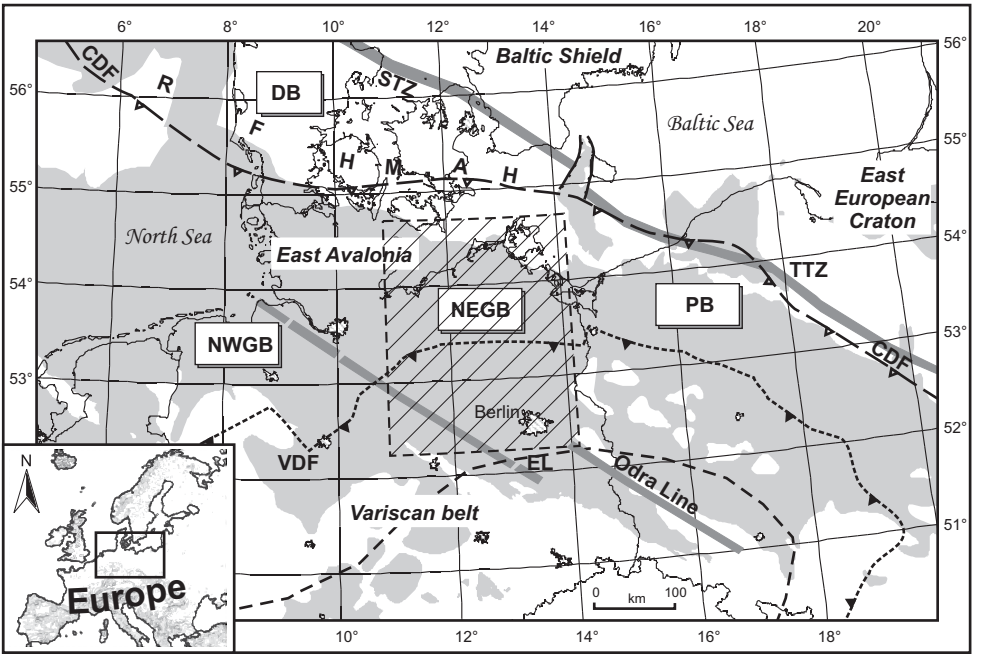
6°
8°
10°
12°
14°
16°
18°
20°
56°
55°
54°
53°
52°
51°
CDF
R
F
H
M
A
H
STZ
DB
Baltic Shield
Baltic Sea
East
European
Craton
North Sea
East Avalonia
NEGB
PB
TTZ
CDF
NWGB
Berlin
VDF
EL
Odra Line
Variscan belt
0
km
100
N
Europe

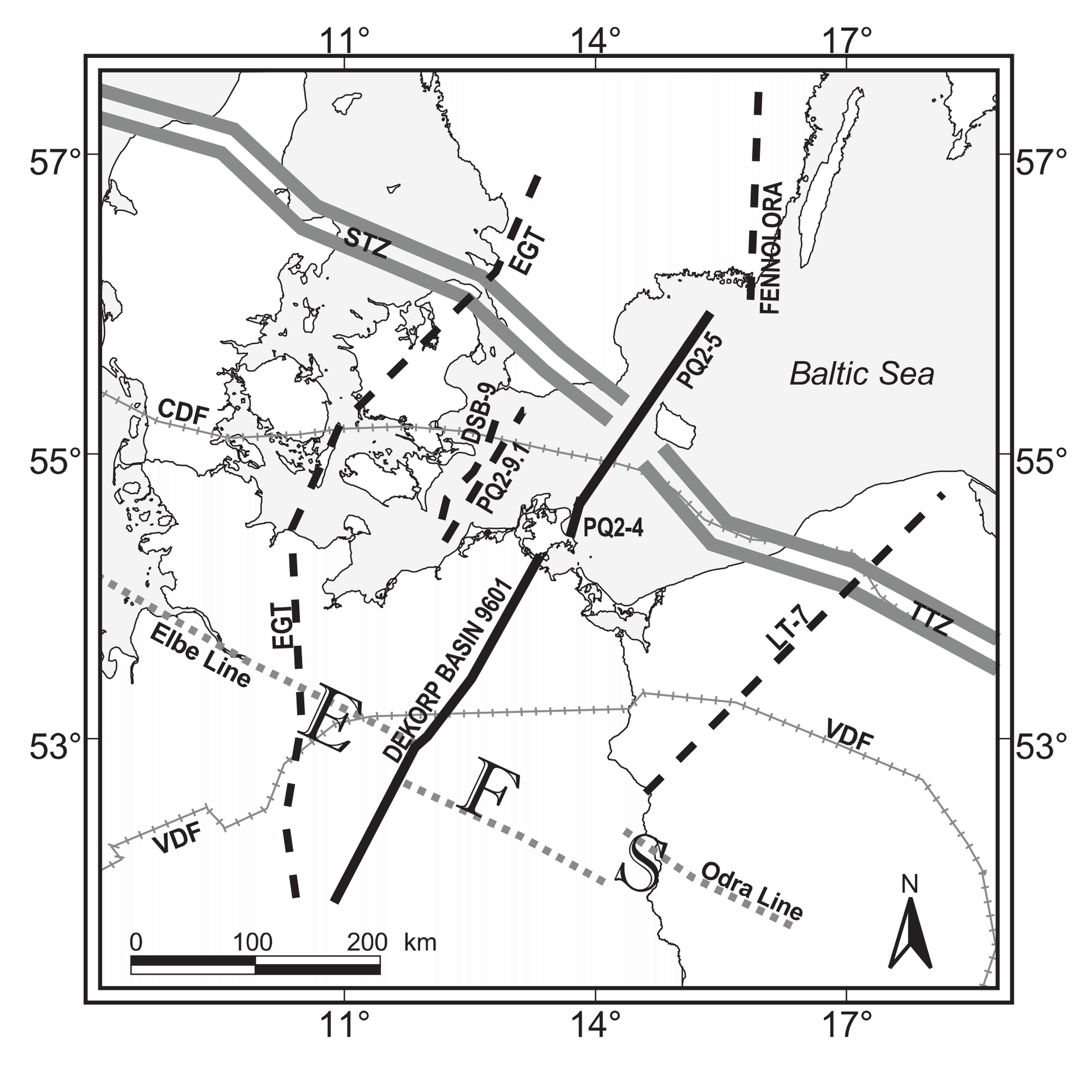
11°
14°
17°
57°
55°
53°
STZ
EGT
FENNOLORA
PQ2-5
Baltic Sea
CDF
DSB-9
PQ2-9.1
PQ2-4
TTZ
Elbe Line
EGT
DEKORP BASIN 9601
T-7
VDF
VDF
Odra Line
N
0
100
200 km

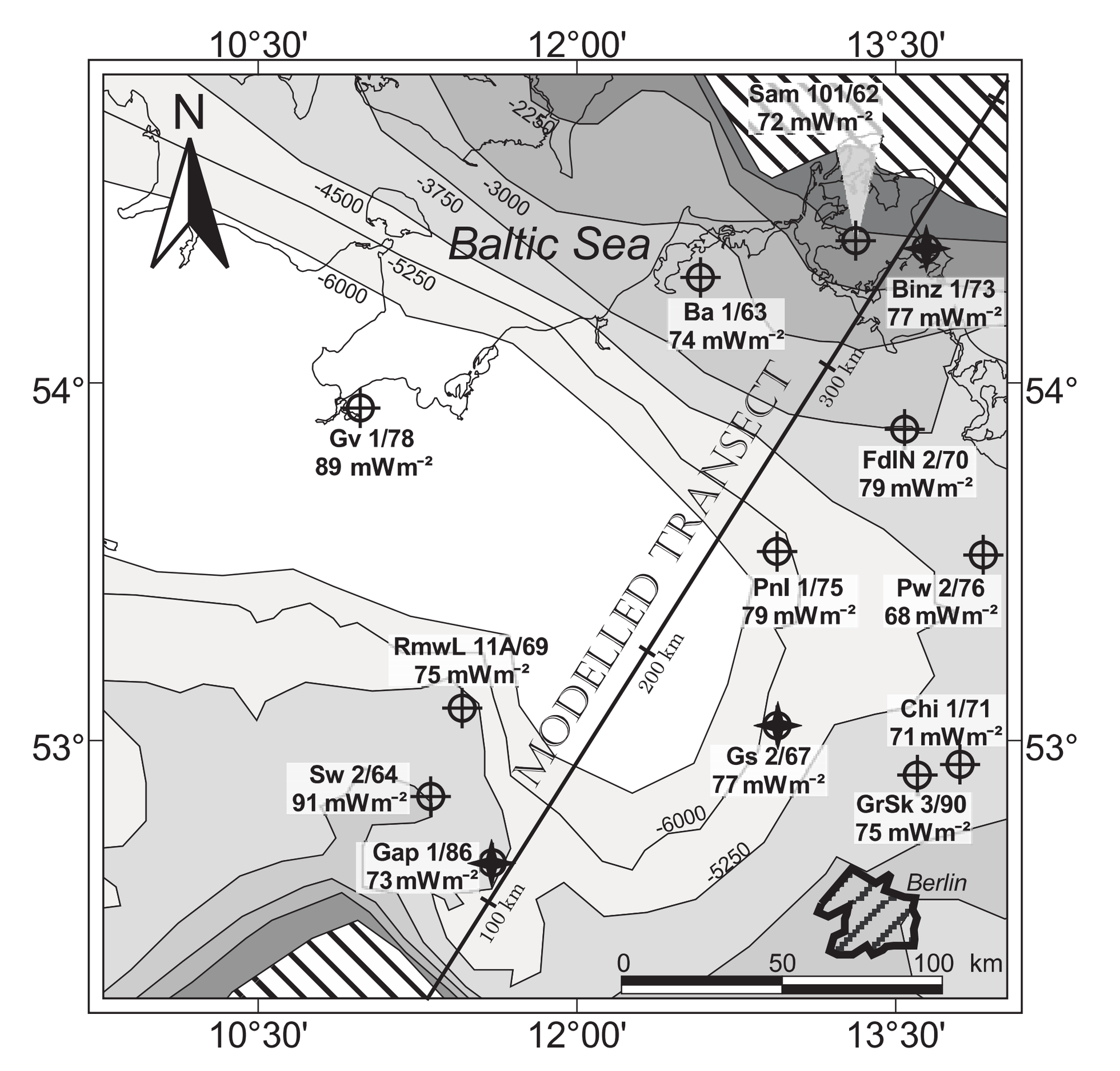
10°30'
12°00'
13°30'
54°
53°
N
Baltic Sea
-2250
-3000
-3750
-4500
-5250
-6000
Sam 101/62
72 mWm⁻²
Binz 1/73
77 mWm⁻²
Ba 1/63
74 mWm⁻²
Gv 1/78
89 mWm⁻²
FdlN 2/70
79 mWm⁻²
MODELLED TRANSECT
300 km
200 km
100 km
Pnl 1/75
79 mWm⁻²
Pw 2/76
68 mWm⁻²
RmwL 11A/69
75 mWm⁻²
Chi 1/71
71 mWm⁻²
Gs 2/67
77 mWm⁻²
Sw 2/64
91 mWm⁻²
GrSk 3/90
75 mWm⁻²
Gap 1/86
73 mWm⁻²
Berlin
0
50
100 km

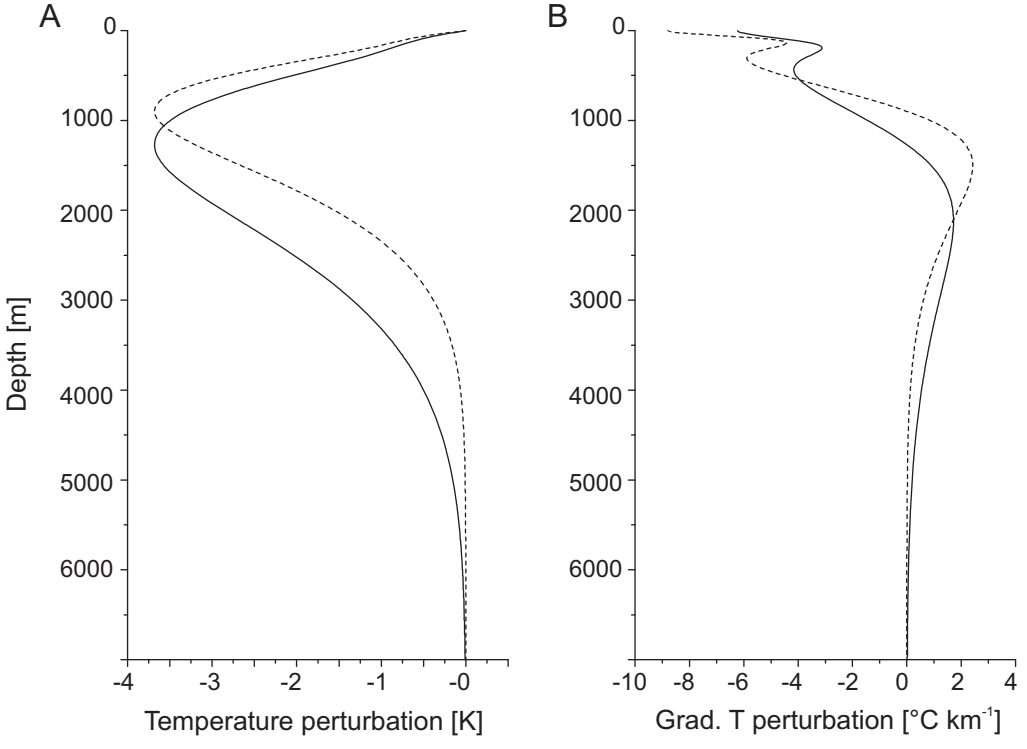
A
B
Depth [m]
0
1000
2000
3000
4000
5000
6000
-4
-3
-2
-1
-0
Temperature perturbation [K]
-10
-8
-6
-4
-2
0
2
4
Grad. T perturbation [°C km-1]

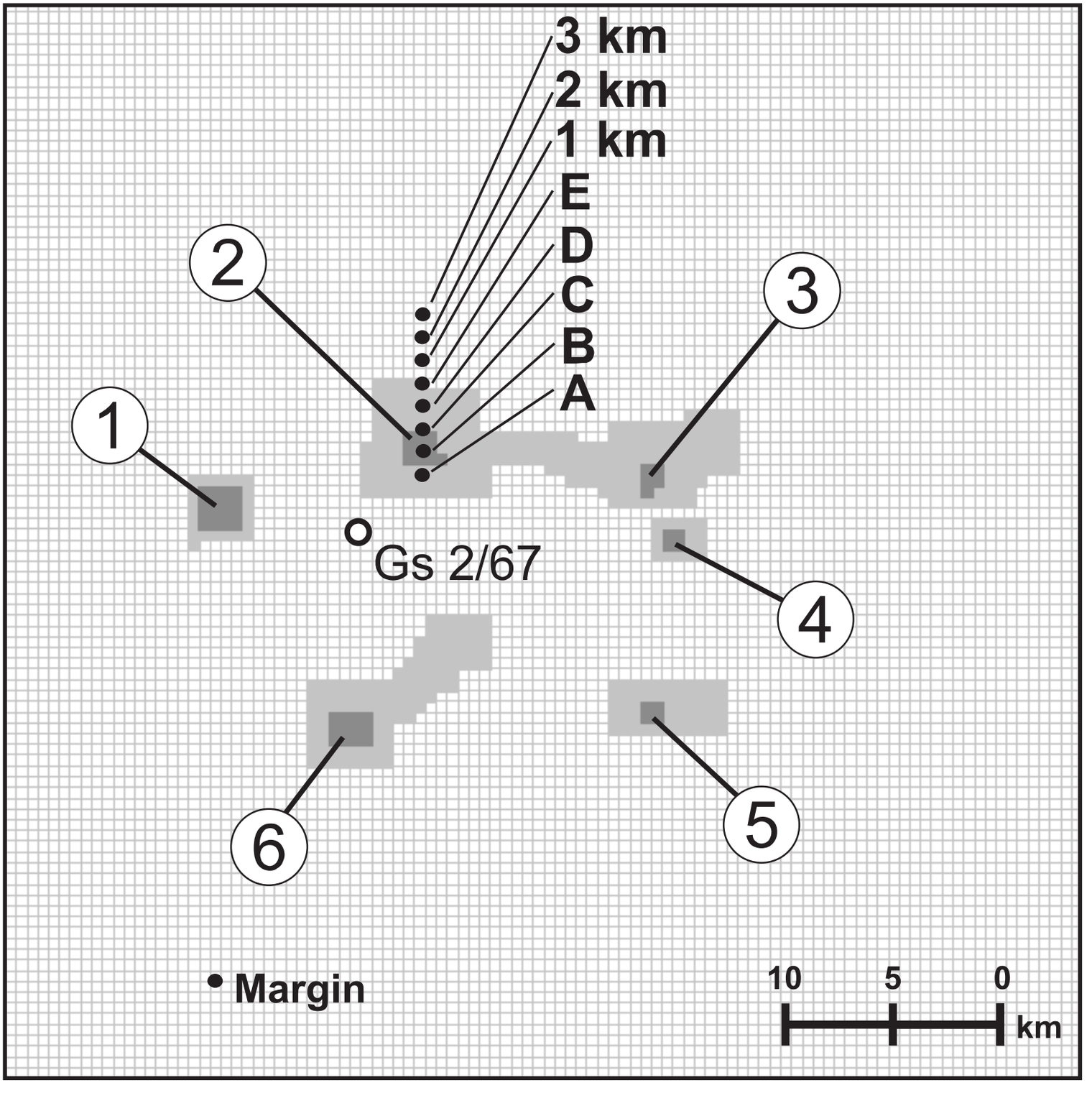
3 km
2 km
1 km
E
D
C
B
A
1
2
3
4
5
6
Gs 2/67
Margin
10
5
0
km

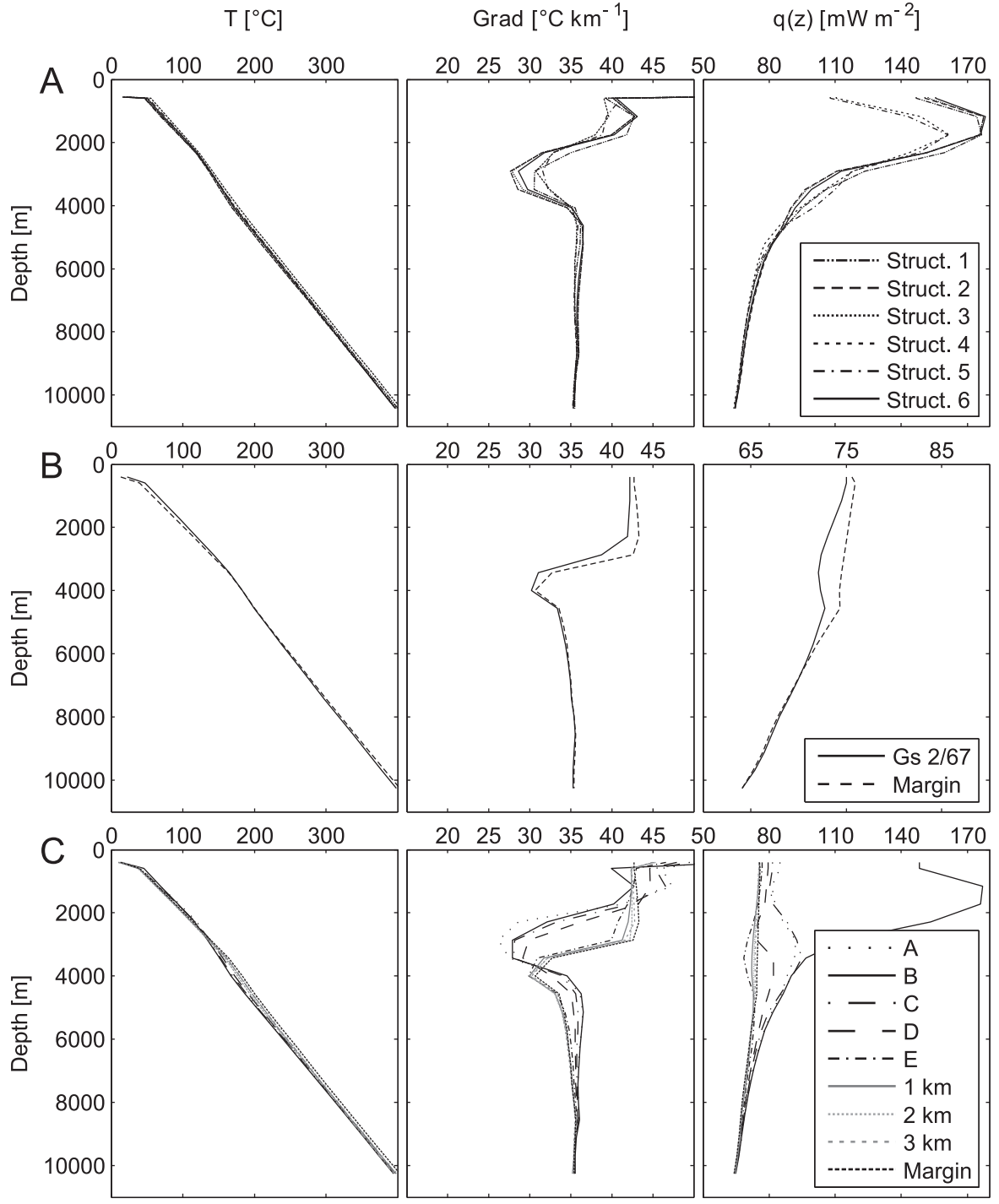
T [°C]
Grad [°C km^{-1}]
q(z) [mW m^{-2}]
A
B
C
Depth [m]
0
2000
4000
6000
8000
10000
Struct. 1
Struct. 2
Struct. 3
Struct. 4
Struct. 5
Struct. 6
Gs 2/67
Margin
A
B
C
D
E
1 km
2 km
3 km
Margin

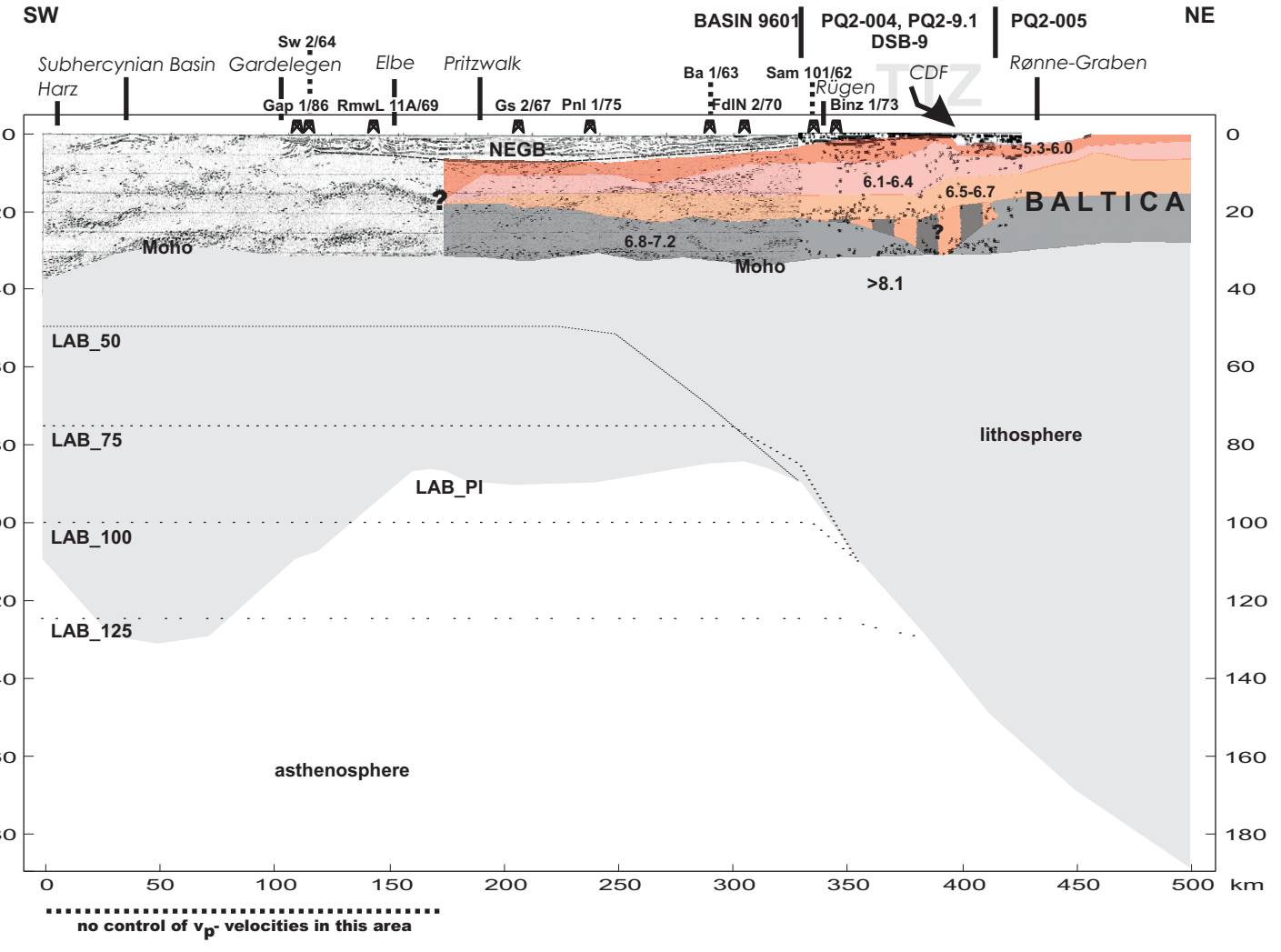
SW
NE
BASIN 9601
PQ2-004, PQ2-9.1
DSB-9
PQ2-005
Subhercynian Basin
Harz
Gardelegen
Sw 2/64
Elbe
Pritzwalk
Ba 1/63
Sam 101/62
Rügen
CDF
TTZ
Rønne-Graben
Gap 1/86
RmwL 11A/69
Gs 2/67
Pnl 1/75
FdlN 2/70
Binz 1/73
NEGB
5.3-6.0
6.1-6.4
6.5-6.7
BALTICA
Moho
6.8-7.2
Moho
>8.1
LAB_50
LAB_75
LAB_Pl
LAB_100
LAB_125
lithosphere
asthenosphere
0
20
40
60
80
100
120
140
160
180
0
50
100
150
200
250
300
350
400
450
500
km
no control of v_p- velocities in this area

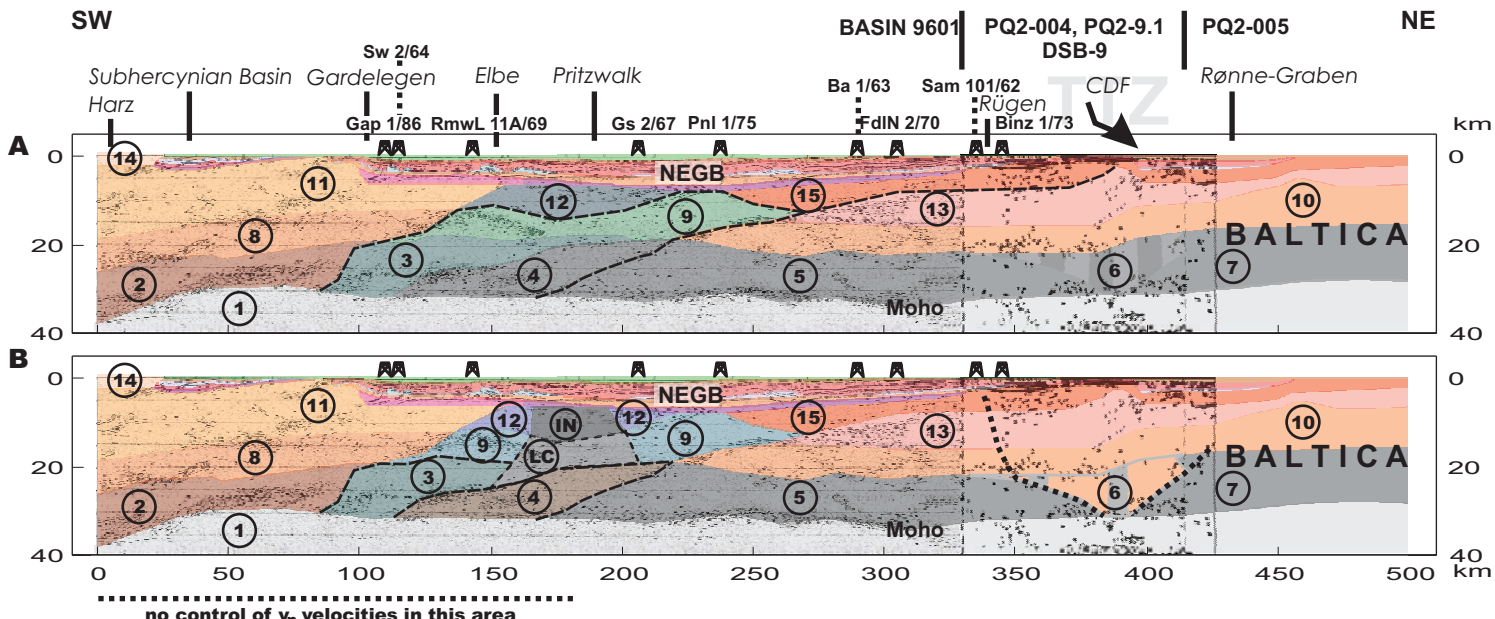
SW
NE
BASIN 9601
PQ2-004, PQ2-9.1
DSB-9
PQ2-005
Subhercynian Basin
Harz
Gardelegen
Sw 2/64
Elbe
Pritzwalk
Ba 1/63
Sam 101/62
Rügen
CDF
TTZ
Rønne-Graben
Gap 1/86
RmwL 11A/69
Gs 2/67
Pnl 1/75
FdlN 2/70
Binz 1/73
km
A
B
NEGB
BALTICA
Moho
IN
LC
no control of v_p velocities in this area

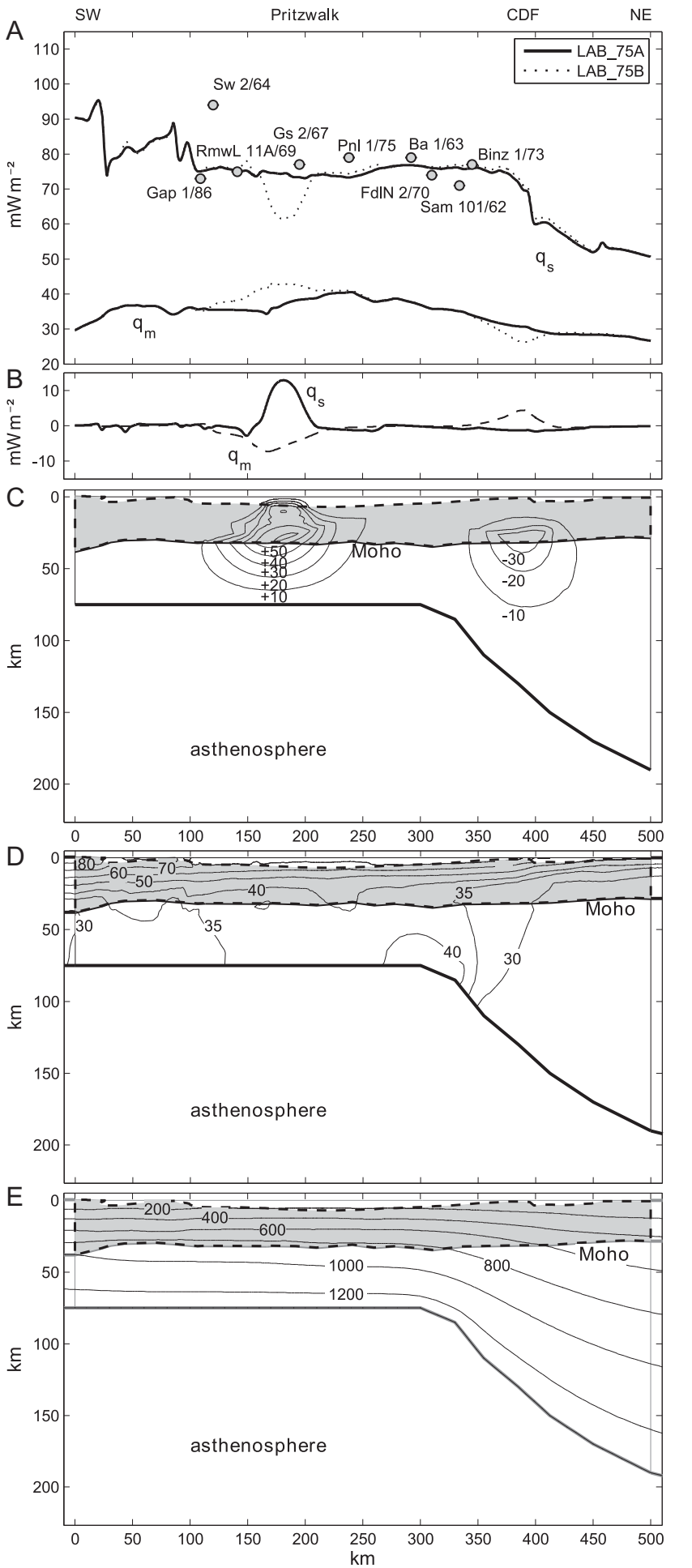
SW
Pritzwalk
CDF
NE
A
LAB_75A
LAB_75B
Sw 2/64
Gs 2/67
RmwL 11A/69
PnI 1/75
Ba 1/63
Binz 1/73
Gap 1/86
FdIN 2/70
Sam 101/62
mW m⁻²
q_s
q_m
B
C
Moho
+50
+40
+30
+20
+10
-30
-20
-10
km
asthenosphere
D
80
70
60
50
40
35
30
Moho
asthenosphere
E
200
400
600
800
1000
1200
Moho
asthenosphere
km

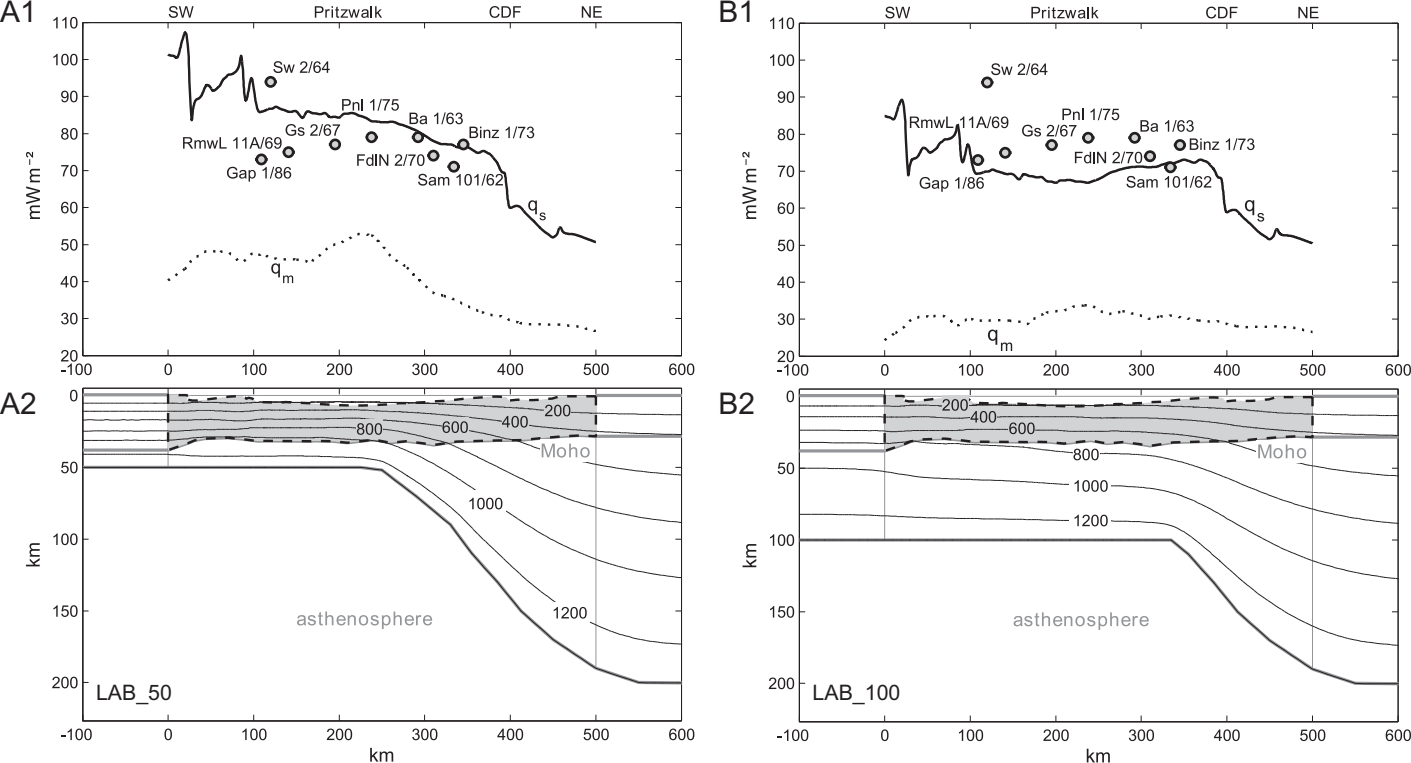
A1
SW
Pritzwalk
CDF
NE
mW m⁻²
Sw 2/64
PnI 1/75
Ba 1/63
Gs 2/67
Binz 1/73
RmwL 11A/69
FdlN 2/70
Gap 1/86
Sam 101/62
q_s
q_m
A2
km
200
400
600
800
Moho
1000
1200
asthenosphere
LAB_50
B1
B2
LAB_100

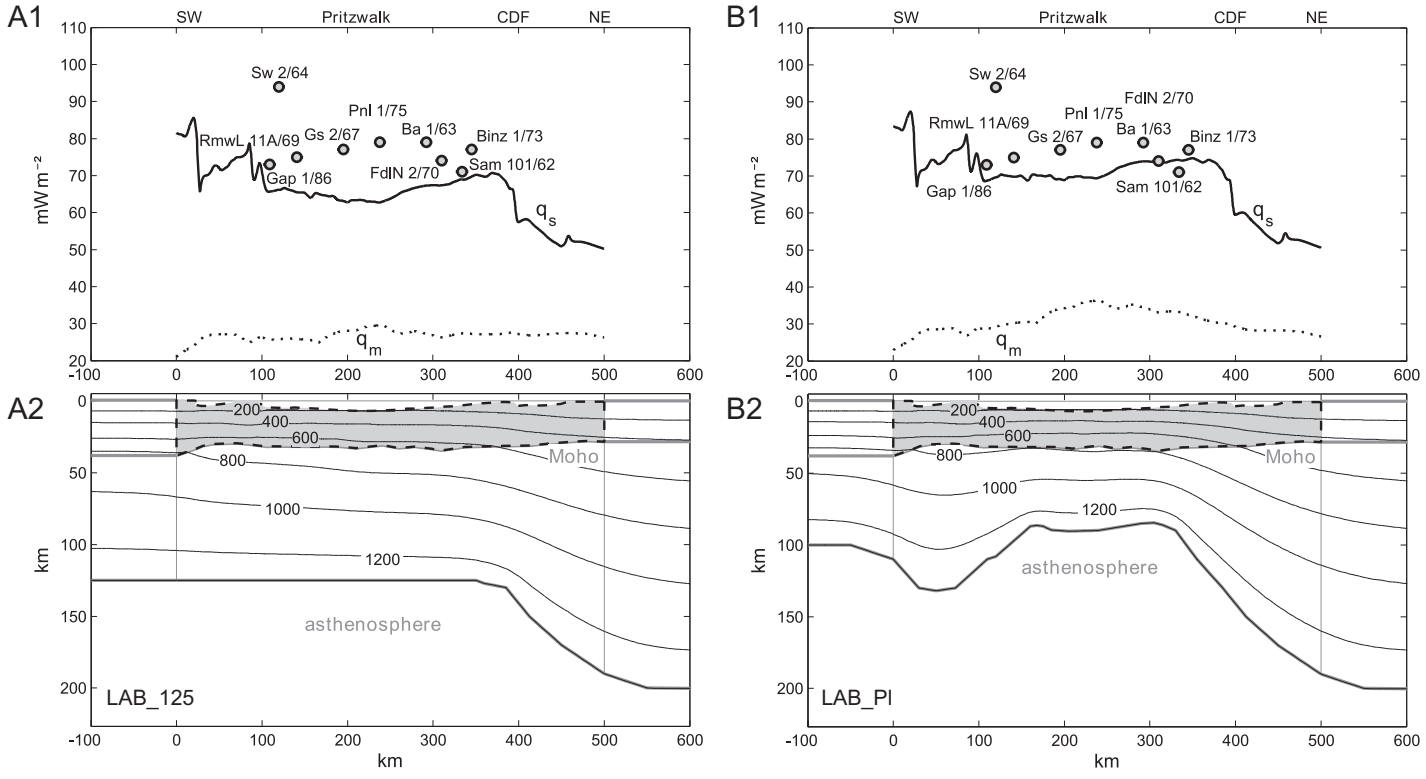
A1
SW
Pritzwalk
CDF
NE
Sw 2/64
RmwL 11A/69
Gap 1/86
Gs 2/67
PnI 1/75
FdlN 2/70
Ba 1/63
Binz 1/73
Sam 101/62
q_s
q_m
mW m^{-2}
A2
200
400
600
800
1000
1200
Moho
asthenosphere
LAB_125
km
B1
SW
Pritzwalk
CDF
NE
Sw 2/64
RmwL 11A/69
Gap 1/86
Gs 2/67
PnI 1/75
FdlN 2/70
Ba 1/63
Binz 1/73
Sam 101/62
q_s
q_m
mW m^{-2}
B2
200
400
600
800
1000
1200
Moho
asthenosphere
LAB_PI
km

Borehole location	Long. E	Lat. N	T-log Qual.	Depth interval Top [m b.g.l.]	Depth interval Bottom [m b.g.l.]	Stratigraphy	Main Lithology	Temperature Top [°C]	Temperature Bottom [°C]	Grad. T uncorr.	Grad. T corr.	λ of interval [$Wm^{-1}K^{-1}$]	In-situ λ [$Wm^{-1}K^{-1}$]	q [mWm^{-2}]	q_{mean} [mWm^{-2}]	q(A) [mWm^{-2}]	q_s [mWm^{-2}]
GrSk 3/90	13°36'	52°54'	A	2800	3770	Permian (Zechstein, Staßfurt)	SALT	119.9	135.1	15.8 ± 0.0	-	5.2 ± 0.4	3.9 ± 0.2	61.7 ± 3.2			
				4230	4286	Permo-Carboniferous	VOLC	148.6	150.8	40.1 ± 0.0	-	2.2 ± 0.1	2.0 ± 0.1	79.3 ± 4.1	70.5 ± 2.9	4.2 ± 0.8	75 ± 3
Gs 2/67	12°56'	53°2'	B	4100	4150	Permian (Zechstein)	ANHY, SALT	156.8	157.9	22.0 ± 0.0	-	4.9 ± 0.4	3.5 ± 0.2	77.0 ± 4.4			
				4200	4600	Permian (Elbe Subgroup)	SLST, SDST	159.0	170.0	28.5 ± 1.0	-	3.2 ± 0.2	2.6 ± 0.1	72.6 ± 4.8			
				4650	4750	Permian (Havel Subgroup)	SDST, SLST	171.1	173.2	21.0 ± 0.6	-	4.2 ± 0.3	3.0 ± 0.2	64.5 ± 4.2			
				4800	5000	Permian (Altmark Subgroup?)	VOLC, SLST	174.8	181.0	31.2 ± 1.5	-	2.7 ± 0.3	2.2 ± 0.2	69.9 ± 6.6	71.1 ± 3.2	5.9 ± 1.2	77 ± 3
RmwL 11A/69	11°28'	53°5'	B	500	750	Permian (Zechstein)	SALT, ANHY	36.2	42.3	24.5 ± 0.5	-	5.0 ± 0.4	4.7 ± 0.4	(115.7 ± 10.1)			
				1700	1950	Permian (Zechstein)	SALT, ANHY	67.6	75.2	31.2 ± 0.7	-	4.9 ± 0.5	4.2 ± 0.4	(131.4 ± 13.1)			
				3200	3450	Permian (Zechstein)	SALT, ANHY	107.3	113.0	22.9 ± 0.5	-	5.2 ± 0.4	4.0 ± 0.3	(92.3 ± 6.2)			
				3500	4250	Permian (Elbe S., Havel S.)	SDST, MDST	114.3	139.8	34.2 ± 0.4	-	3.1 ± 0.2	2.6 ± 0.2	(89.9 ± 5.9)	*	*	0.5 ± 0.1	*75 ± 5
Sam 101/62	13°19'	54°23'	B	1450	1700	Permian (Zechstein)	ANHY, SALT	48.3	52.2	15.5 ± 0.5	-	5.0 ± 0.5	4.5 ± 0.5	70.2 ± 7.6			
				1800	1950	Permo-Carboniferous	VOLC	54.6	59.0	29.6 ± 2.6	-	2.5 ± 0.5	2.4 ± 0.5	70.7 ± 16.0	70.5 ± 8.8	1.8 ± 0.4	72 ± 9
Ba 1/63	12°35'	54°17'	C	2300	2800	Permian (Zechstein, Staßfurt)	SALT	86.0	93.7	15.3 ± 0.1	-	5.2 ± 0.4	4.3 ± 0.3	64.8 ± 4.6			
				2900	3100	Permian (Elbe Subgroup)	SLST, SDST	95.5	101.8	31.8 ± 0.6	-	2.9 ± 0.3	2.6 ± 0.3	82.0 ± 8.4			
				3200	3500	Permo-Carboniferous	VOLC	105.7	111.2	27.3 ± 0.3	-	2.5 ± 0.2	2.3 ± 0.2	61.9 ± 4.4			
				3550	4500	Carboniferous	SLST, SDST	114.2	138.4	25.5 ± 0.1	-	3.7 ± 0.2	3.0 ± 0.2	77.3 ± 4.4			
				4550	4750	Carboniferous	MGRA	139.5	143.6	20.4 ± 0.3	-	3.3 ± 0.2	2.7 ± 0.2	(55.5± 3.6)	71.1 ± 3.5	3.1 ± 0.6	74 ± 4
Chi 1/71	13°48'	52°56'	C	2900	3650	Permian (Zechstein, Staßfurt)	SALT	126.6	139.8	17.8 ± 0.2	-	5.2 ± 0.4	3.8 ± 0.2	68.3 ± 4.3	68.3 ± 4.3	3.0 ± 0.6	71 ± 4
Pw 2/75	13°55'	53°31'	C	2950	3900	Permian (Zechstein, Staßfurt)	SALT	116.0	128.5	13.1 ± 0.1	-	5.2 ± 0.4	3.9 ± 0.2	51.1 ± 2.6			
				4050	4300	Permian (Elbe Subgroup)	MDST, SDST	131.6	139.5	32.8 ± 1.2	-	3.2 ± 0.2	2.3 ± 0.1	76.4 ± 3.8	63.8 ± 2.3	4.0 ± 0.8	68 ± 2
Sw 2/64	11°19'	52°50'	C	2850	3000	Permian (Zechstein, Leine)	SALT	122.6	126.5	25.0 ± 2.7	-	5.1 ± 0.3	3.8 ± 0.2	95.8 ± 11.1			
				3150	3250	Permian (Zechstein, Staßfurt)	SALT	129.2	131.1	19.0 ± 2.9	-	5.2 ± 0.4	3.9 ± 0.2	73.2 ± 12.0			
				3350	3650	Permian (Elbe Subgroup)	SDST, MDST	133.0	142.6	32.7 ± 0.7	-	3.5 ± 0.2	2.8 ± 0.2	92.9 ± 5.3	87.3 ± 5.7	3.5 ± 0.7	91 ± 6
Binz 1/73	13°38'	54°23'	D	1450	1550	Permo-Carboniferous	VOLC	53.0	54.9	19.0 ± 0.6	23.6 ± 2.0	2.9 ± 0.2	2.8 ± 0.2	66.1 ± 7.3			
				1600	1900	Carboniferous (Stephanian)	SDST, MDST	55.4	60.6	17.4 ± 0.6	22.0 ± 2.0	3.9 ± 0.2	3.6 ± 0.2	79.2 ± 8.4			
				1950	2750	Carboniferous (Westphalian)	MDST, SDST	61.6	79.1	21.9 ± 0.3	21.9 ± 1.0	3.8 ± 0.2	3.4 ± 0.2	74.5 ± 5.5			
				2800	3150	Upper Devonian (Frasnian)	CLMD, MDST	80.5	92.1	33.8 ± 0.8	35.9 ± 2.0	2.6 ± 0.2	2.4 ± 0.2	86.2 ± 8.6			
				3200	3750	Middle Devonian (Givetian)	SDST, SLST	92.8	103.2	19.1 ± 0.6	21.2 ± 2.0	4.2 ± 0.2	3.5 ± 0.2	75.0 ± 8.2			
				3800	4200	Middle Devonian (Eifelian-Givetian)	SDST, SLST	103.3	110.6	19.7 ± 1.0	21.8 ± 3.0	4.1 ± 0.2	3.4 ± 0.2	74.1 ± 11.1			
				4250	5000	Middle Devonian (Eifelian)	SLST, SDST	111.3	126.4	20.1 ± 6.0	22.2 ± 6.0	3.9 ± 0.2	3.2 ± 0.2	71.0 ± 19.7	75.2 ± 4.1	1.5 ± 0.3	77 ± 4
Gap 1/86	11°36'	52°39'	D	3400	3800	Permian (Zechstein)	ANHY, SALT	125.0	131.0	13.6 ± 1.0	16.1 ± 2.0	4.8 ± 0.2	3.7 ± 0.1	59.6 ± 7.6			
				3850	4150	Permian (Elbe Subgroup)	SDST, SLST	131.7	138.2	22.2 ± 0.6	24.7 ± 2.0	3.5 ± 0.2	2.9 ± 0.2	71.6 ± 7.6			
				4200	4350	Permian (Havel Subgroup)	SDST	139.2	142.2	20.6 ± 1.3	23.1 ± 2.0	4.3 ± 0.4	3.3 ± 0.3	76.2 ± 9.6			
				4400	4500	Permo-Carboniferous	BASA	143.7	149.7	32.4 ± 2.4	34.9 ± 3.0	2.2 ± 0.2	2.0 ± 0.2	68.4 ± 9.1	69.0 ± 4.2	4.2 ± 0.8	73 ± 4
FdlN 2/70	13°33'	53°52'	D	3050	3400	Permian (Zechstein, Staßfurt)	SALT	120.4	126.8	18.4 ± 0.2	20.0 ± 2.0	5.2 ± 0.4	3.8 ± 0.1	75.8 ± 7.8			
				3600	3750	Permian (Elbe Subgroup)	CONG	130.1	134.0	26.6 ± 1.3	28.2 ± 2.0	3.2 ± 0.2	2.7 ± 0.2	74.7 ± 7.7	75.2 ± 5.5	3.7 ± 0.7	79 ± 6
Pnl 1/75	12°56'	53°32'	D	4350	4500	Permian (Zechstein, Staßfurt)	SALT	147.7	150.7	19.8 ± 3.9	23.5 ± 4.0	5.2 ± 0.4	3.6 ± 0.1	(83.2± 14.4)			
				4600	5050	Permian (Elbe Subgroup)	SLST, SDST	153.0	165.5	26.9 ± 0.3	29.6 ± 2.0	3.1 ± 0.2	2.5 ± 0.1	74.0 ± 5.8	74.0 ± 5.8	4.7 ± 0.9	79 ± 6
Gv 1/78	10°59'	53°56'	D	4600	4800	Permian (Zechstein, Staßfurt)	SALT	137.0	141.0	20.0 ± 1.7	21.6 ± 2.0	5.2 ± 0.4	3.8 ± 0.2	82.1 ± 8.7	82.1 ± 8.7	6.6 ± 1.3	89 ± 9

T-log Qual. refers to different quality categories of temperature logs: A, high-precision, high-resolution, and unperturbed temperatures; B, unpertubed temperatures; C, slightly perturbed temperatures, not corrected; D, moderately perturbed temperatures, corrected. *Grad. T uncorr.* is uncorrected interval temperature gradient; *Grad. T corr.* is interval temperature gradient corrected for drilling effects. λ is interval thermal conductivity based on values from Lotz (2004) and Norden and Förster (2006). Values for Permian Zechstein rocks are from Kopietz et al. (1995). *In-situ* λ is thermal conductivity corrected for in-situ temperature. *q* is interval heat flow. q_{mean} is mean heat flow from different intervals. *q(A)* is the heat flow budget of the overburden, above the heat flow interval. *qs* is surface heat flow sensu strico. Values in brackets were not regarded for the calculation of q_{mean}. * q_{mean} not meaningful due to heat refraction; q_s was estimated according to thermal modelling (see text).

Lithological abbreviations: BASA basaltoid, CLMD calcareous mudstone, CONG conglomerate, MDST mudstone, MGRA microgranite, SDST sandstone, SLST siltstone, VOLC volcanic rock.

Zone	Description	Thickness [m]	λ [$Wm^{-1}K^{-1}$]	A [Wm^{-3}]
1	Top zone	500	1.5	0
2	Intermediate zone	0-4000	1.8	0.5×10^{-6}
3	Salt	500-4000	5	0
4	Base zone, below salt	6500	2.9	1.8×10^{-6}

A

Stratigraphy / unit	Polygon	Major rock type	λ [$Wm^{-1}K^{-1}$]	λ correction T	λ correction p	A [μWm^{-3}]	Density [10^3 kgm^{-3}]
Quaternary to Upp. Cretaceous		sandstone, mudstone, limestone	1.8	7	-	0.90	2.10
Lower Cretaceous		sandstone/siltstone	2.0	7	-	1.50	2.30
Jurassic-Triassic		sandstone/mudstone	2.2	7	-	1.60	2.54
Zechstein		evaporites	4.5	7	-	0.40	2.16
Rotliegend, sedimentary		sandstone/mudstone	3.3	7	-	1.50	2.60
Permo-Carboniferous, magmatic		volcanic rocks	2.5	7	-	2.00-3.40	2.65
"Upper crust"	15	granite/granodiorite	3.1	3	+	2.80	2.65
	14	granite/granodiorite	3.3	3	+	3.00	2.70
	13	diorite-parametamorphic rock	2.9	3	+	2.30	2.65
	12	quartz phyllite?	2.7	6	+	2.00	2.80
	11	granite/granodiorite	3.1	3	+	2.00	2.70
	10	intermediate granulite?	2.7	1	+	0.80	2.77
	9	mica schist?	2.7	6	+	1.80	2.85
	8	paragneiss	2.9	6	+	1.90	2.75
"Lower crust"	7	plagioclase-rich mafic granulite	2.0	2	+	0.10	2.90
	6	mafic granulite	2.2	2	+	0.10	2.90
	5	garnet/pyroxene-rich mafic granulite	2.3	2	+	0.10	3.00
	4	basalt	2.0	5	+	0.40	3.00
	3	felsic granulite	2.7	1	+	0.80	2.80
	2	granulite?	2.3	1	+	0.60	2.85
Lithospheric mantle	1	peridotite	4.1	4	+	0.01	3.30

B

Unit	Polygon	Major rock type	λ [$Wm^{-1}K^{-1}$]	λ correction T	λ correction p	A [μWm^{-3}]	Density [10^3 kgm^{-3}]
"Upper crust"	12	granite/granodiorite	3.1	3	+	2.50	2.70
	9	paragneiss	2.9	6	+	2.10	2.75
Intrusion	IN	basalt	2.0	5	+	0.40	2.95
"Lower crust"	6	felsic granulite	2.7	1	+	0.80	2.80
	4/LC	mafic granulite?	2.2	2	+	0.10	3.10

Polygon numbering as in Figure 8. λ reflects laboratory conditions (25°C, atmospheric pressure). λ *correction* was made for temperature (T) and pressure (p, marked with +). T-correction numbers 1-6 refer to categories by Seipold (2001): 1 felsic granulite, 2 mafic granulite, 3 granite, 4 peridotite, 5 amphibolite, and 6 gneiss; category 7 refers to sediments after Somerton (1992). Pressure correction was made for polygons in the upper and lower crust and lithospheric mantle using $\lambda = \lambda_0 (1+\alpha p)$ from Seipold (2001). A refers to radiogenic heat production. Density in model **A** is after Lassen et al. (2002); density in model **B** is after Kuder (2002).

Crustal scenario at location:		HFD mW m^{-2}	Temp Moho °C	Depth LAB km	q_{crust} mW m^{-2}	q_m mW m^{-2}
Gap 1/86	min.	74	802	99		
73 mW m^{-2}		**77**	**855**	**85**	45	32
	max.	80	903	75		
Gs 2/67	min.	74	870	74		
77 mW m^{-2}		**77**	**923**	**66**	36	41
	max.	80	972	59		
Binz 1/73	min.	74	687	111		
77 mW m^{-2}		**77**	**740**	**96**	43	34
	max.	80	792	85		